

Following the reviewers' thoughtful comments and suggestions, we have carefully revised the manuscript. Compared to the earlier version, the main changes are as follows:

1) We have re-run the entire assimilation using improved segmentation methods. In the previous version, we did split the period into segments of 14 months with a 2-month overlap between adjacent years in order to save computational time. We thought that this approach would not influence the inverted flux trends under the assumption that the initial conditions for each segment are properly optimized by the system with just 2 months of overlap, a spin-up time that is about the lifetime of CO in the atmosphere. Under closer scrutiny, it appears that this segmentation actually generates a small discontinuity in the concentration time series that affects some regional signals. Therefore, we have re-run the inversion with only three segments and with an overlap of 4 months between adjacent segments with initial conditions optimized upstream. Figures are systematically updated and parts of the results are revised, but the main conclusions are not affected.

2) Following reviewers' suggestion, we added one table to summarize regional CO concentration trends in the total column and surface boundary layer from observations and corresponding prior/posterior modelling (Table 2). We also added one table to summarize the model misfit to CH₄ and MCF observations that are assimilated jointly in the system (Table 3). In addition, we converted the units for MOPITT column retrievals from molec cm⁻² to ppb. Thus there are considerable edits in terms of numbers and units in Section 3, but the main results are not changed.

3) We added one figure to show the horizontal and vertical distribution of the two OH fields: TransCom and INCA (Fig. 3 in the updated version). In the meantime, we removed one figure - the old Fig. 4 showing the latitudinal mean bias of prior/posterior CO concentration compared to surface in-situ measurements, because this information is now summarized in Table 2.

Detailed responses to each question and comment from the reviewers are attached below. The manuscript with all editing tracked is also attached after the response.

The co-authors
27/10/2015

Reply to Referee #1

We thank the reviewer for his/her thoughtful comments and valuable suggestions. We have addressed all the issues raised in the review. The full review is copied hereafter in blue and our responses are inserted where appropriate.

Anonymous Referee #1

This paper uses as data-assimilation framework to infer CO emissions from satellite observations. The CO inversion system is coupled to CH₂O, CH₄, and MCF, which provide constraints on the sources and sinks of CO. The target period of the study is a full decade (2002-2011). The study has the aim to provide a consistent analysis of the drivers of the observed decline in CO total columns from MOPITT (figure 3). Although the paper is relative convincing in some aspects, some inconsistencies are also apparent, which need to be better explained or analyzed. Below, these are listed under major issues.

We thank the reviewer for pointing out some elements that we did not articulate well enough in the previous version of the manuscript. We hope that this reply clarifies these issues.

Major issues

1. Is the system well balanced?

The focus of this paper is on CO, but also CH₄ and MCF measurements are assimilated. One of the burning questions around today is the role of OH, and a possible trend in OH, in the observed CH₄ growth rate changes, exactly in the analyzed period. I was therefore a bit disappointed to find only one sentence: “Similarly for CH₄ and MCF, the inversion fits the assimilated data fairly well, but these results are not shown, as they are not the main focus in this study”. This casts doubts on the added value of the CH₄ and MCF assimilation.

We added a table (Table 3) in the revised paper, which presents the mean model-data bias and the residual root mean squares (RMS) before and after optimization for CH₄ and MCF.

Table 3. Fitness of CH₄ and MCF observations assimilated in the inversion.

Region	OH-type	CH ₄ (ppb)				MCF (ppt)			
		Mean bias		RMS		Mean bias		RMS	
		<i>prior</i>	<i>posterior</i>	<i>prior</i>	<i>posterior</i>	<i>prior</i>	<i>posterior</i>	<i>prior</i>	<i>posterior</i>
NH(30-90)	<i>TransCom</i>	20.6	2.4	749.6	22.2	1.02	-0.02	1.14	0.05
	<i>INCA</i>	-21.0	2.5	658.1	20.1	0.44	-0.09	0.28	0.07
NH(0-30)	<i>TransCom</i>	15.8	1.5	452.6	19.1	0.90	-0.20	0.91	0.16
	<i>INCA</i>	-21.1	-0.1	564.9	13.9	0.40	-0.20	0.21	0.11
SH(0-30)	<i>TransCom</i>	10.9	-2.4	222.1	20.1	1.19	0.09	1.61	0.13
	<i>INCA</i>	-14.3	-4.0	264.9	29.5	0.88	0.23	0.94	0.15
SH(30-90)	<i>TransCom</i>	14.4	0.2	308.3	4.7	0.88	-0.24	0.90	0.17
	<i>INCA</i>	-7.9	-0.4	96.6	5.7	0.60	-0.06	0.46	0.07

The substantial decrease of both the mean bias and RMS reveals the system’s ability to draw information from the CH₄ and MCF observations.

I presume that the cost function consist of a term related to model-data mismatch of MOPITT observations, a background term (emissions of CO, MCF, and CH₄ that deviate significant from the prior), and terms related to CH₄ and MCF misfits at the stations. If such a system is not well balanced, it might be that little of no information is drawn from the MCF and CH₄ misfits. Since the authors claim that they infer no trend in OH they have to verify if their system is adequately set up to detect a possible OH trend. Stating that the inversion fits the MCF observations fairly well is certainly not enough.

Estimating whether the system (or the cost function) is balanced among species is far from trivial. For the prior error covariance matrix **B** and observation error covariance matrix **R**, we assign the error terms separately based on our best knowledge of their uncertainty in the “physical” world based on bottom-up inventories and previous model studies. This is consistent with the Bayesian approach where each information piece brings its own probability density function independent from the other ones: we do not tune the error statistics to artificially balance the weight of each species.

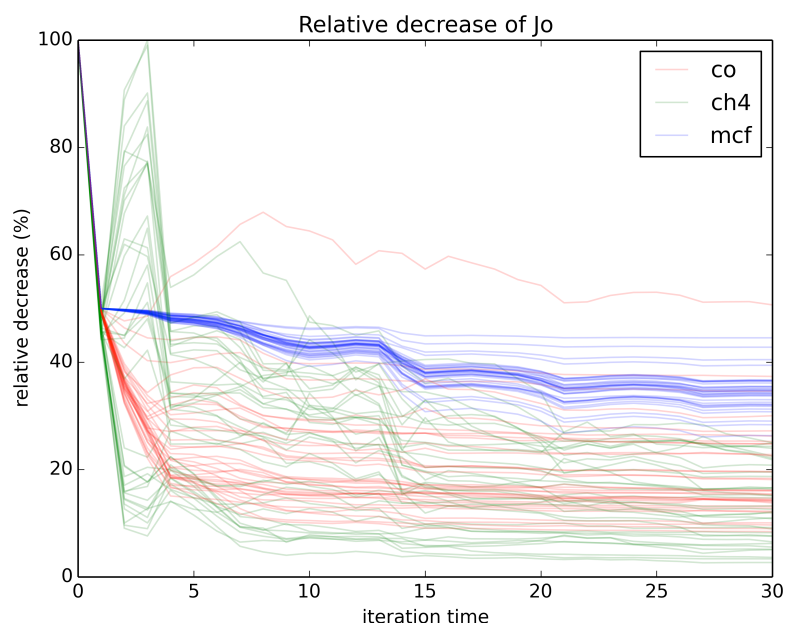
In terms of observation numbers of different species included in the assimilation, which could influence their relative shares in the cost function, MOPITT CO retrievals have higher spatial coverage over the globe so CO has implicitly more observations than CH₄ and MCF. Furthermore, model-data biases could also contribute a potentially large portion of the initial cost function (in our case the model bias is larger for CO than for other species) and we do not think that there is a necessity to “balance among species” in terms of a misfit correction.

Moreover, it would be interesting to present some analysis of the cost function, showing how the optimization changes the cost function, and how CH₄ and MCF observations are used to inform the CO budget in terms of sources and sinks (e.g. by neglecting couplings).

For the reasons stated above, we think that balancing the absolute share of the cost function from each species is not appropriate for the study. Instead, we have analyzed the relative contribution of the three species in the observation term of the cost function during the iterative minimization.

$$J_o = \frac{1}{2} (H(\mathbf{x}) - \mathbf{y})^T \mathbf{R}^{-1} (H(\mathbf{x}) - \mathbf{y})$$

Fig. Relative decrease of J_0 for each species for each year during iteration. CO are shown in red, methane in green and MCF in blue.



In this figure, each line represents the relative decrease in J_0 for one species for a year during each iteration. It shows an efficient decrease compared to the initial cost for all species. For methane (in green) and MCF (in blue) observations at surface station, which are more difficult to represent by the model than satellite CO column retrievals averaged at model resolution (in red), the relative decreases are smaller in some occasions. Nevertheless, the inversion system appears robust at minimizing the cost function.

2. Are the results realistic?

A large fraction of the atmospheric CO comes from the oxidation of NMHCs. Yet, figure 6 shows that large seasonal biases exist with independent satellite observations of CH₂O. This implies that the atmospheric CO sources are also seasonally biased, and these biases will be projected on CO emissions.

We agree that assimilating CH₂O observations could further improve the estimation of CO emissions, in particular to improve the seasonal cycle. It is actually one of our perspectives in this paper. However, the observational data of CH₂O is not fully available for the decade that we study; thus, for the sake of consistency we do not assimilate CH₂O. Instead, the OMI CH₂O retrievals are used as independent evaluation. Fig. 6 of the paper shows, on the one hand, the overall agreement of satellite CH₂O column retrievals with modelled CH₂O concentrations for latitudinal means. On the other hand, it shows that no significant large-scale trends are found in the CH₂O column to contribute to the decrease of CO concentrations that are observed over many regions.

Even more worrying are the large regional emission increments that are presented in

figure 9. For instance, in the region SHSA the emissions are calculated to increase from roughly 50 Tg/yr in 2002 to almost 200 Tg/yr.

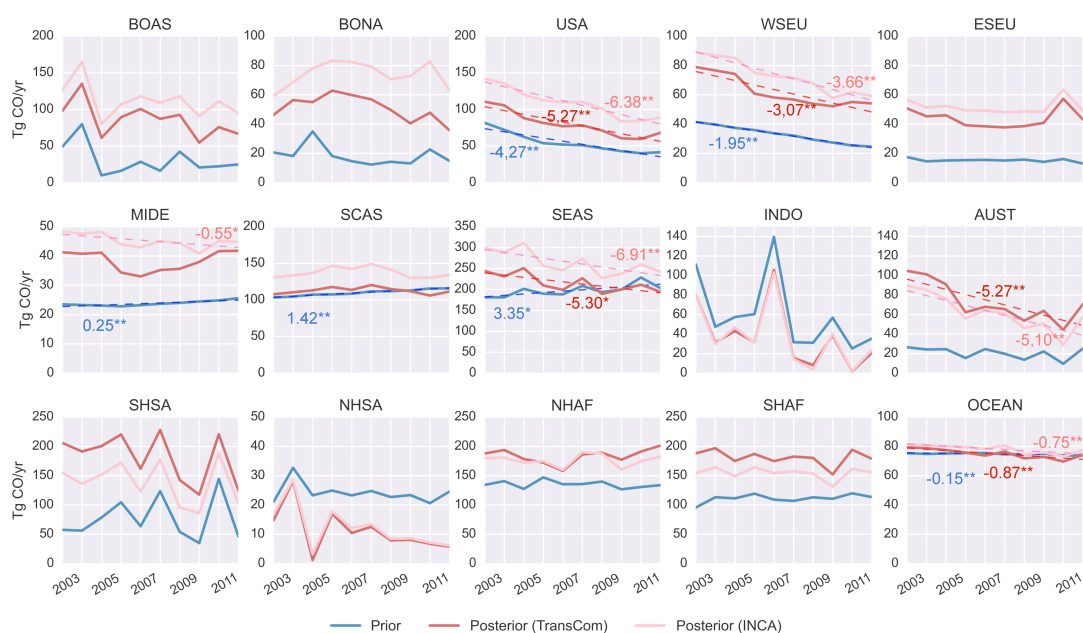
We agree that the relatively large increments in South Hemisphere South America (SHSA) and Australia have large uncertainties due to CH₂O production, OH sink and other factors concerning transport and vertical mixing. However, our study here focuses on the trends of CO emissions, and the uncertainties in terms of regional increments are more systematic than time dependent given the information we gain from OMI CH₂O observations. Therefore, regional increments from the prior to posterior as well as their relative uncertainties are not specifically discussed. Further investigation of this point for a different study will be very interesting.

In later years calculated increments are smaller but the recently described biomass burning year 2007 (Bloom et al., GRL, 2015) visible in the prior seems to disappear in the posterior. Over Australia and Africa also some large increments are calculated. Likely, the two issues are related since CH₂O from isoprene is a major source of CO over SHSA (Stravakou et al., ACPD, 2015).

We thank the reviewer for pointing this out. We traced the problem back to an artefact caused by the way we processed the whole decade in the initial paper. Indeed, for practical reasons, we did split the period into segments of 14 months with a 2-month overlap between adjacent years. We thought that this approach would not influence the inverted flux trends under the assumption that the initial conditions for each segment are properly optimized by the system with just 2 months of overlap, a spin-up time that is about the lifetime of CO in the atmosphere. Under closer scrutiny, it appears that it actually generates a small discontinuity in the concentration time series that affects some regional signals. We have re-run the inversion with only three segments and with an overlap of 4 months between adjacent segments with initial conditions optimized upstream. The main conclusions are not affected, but all figures have been updated.

The updated Fig. 10 is inserted below. High emissions in regions south hemisphere South America (SHSA) and Indonesia (INDO) in the year 2007 are very visible now in the posterior, consistent with the prior and other bottom-up studies.

Fig. 10. Regional annual CO emissions from 2002 to 2011. The prior emissions are shown in blue and the posteriors are shown in red. Dark-red represents posterior with TransCom-OH and pink-red represents posterior with INCA-OH. Linear fit is shown when statistically significant, and slopes are denoted with corresponding colour. * denotes significant at 95% confidence level, and ** denotes significant at 99% confidence level. The notations for the sub-regions are listed below, and the extent of each region is shown in Fig. A1. BOAS - Boreal Asia, BONA - Boreal North America, USA - USA, WSEU – West Europe, ESEU – East Europe, MIDE – Middle East, SCAS – South Central Asia, SEAS – South East Asia, INDO- Indonesia, AUST – Australia, NHSA- North Hemisphere South America, SHSA - South Hemisphere South America, NHAf - North Hemisphere Africa, SHAF – South Hemisphere Africa, OCEAN – all ocean emissions.

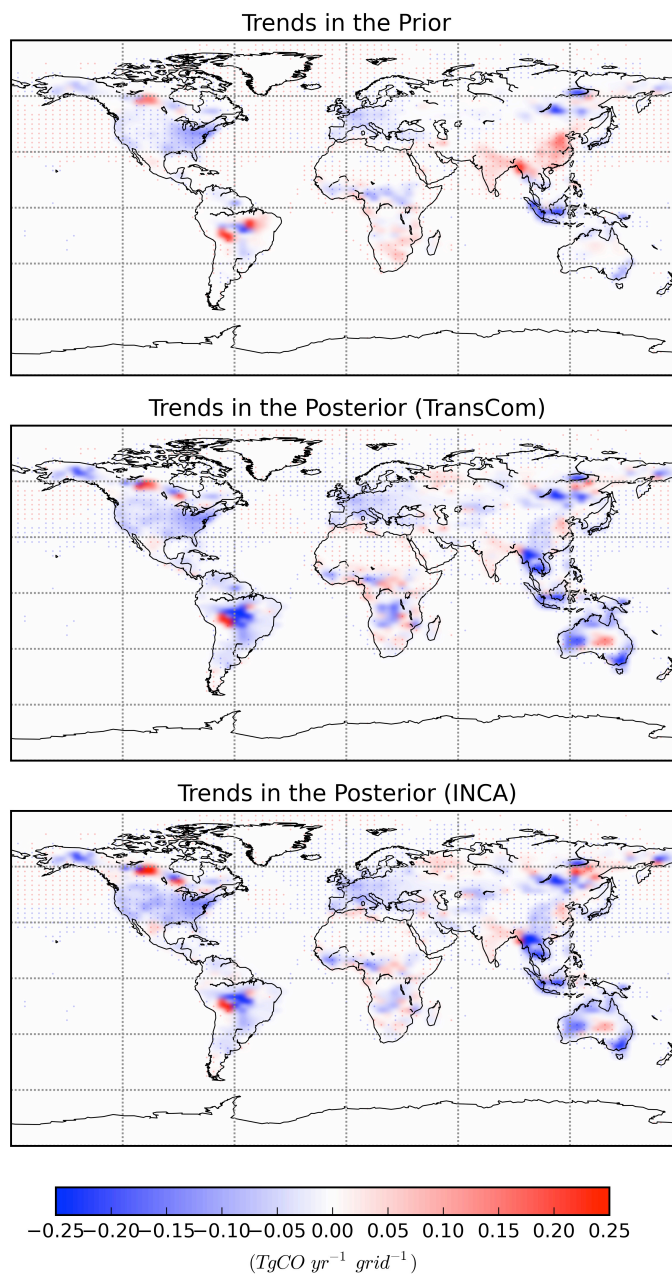


Finally, only the results for the TRANSCOM-OH are shown. These fields have a NH/SH OH ratio closer to 1 and this will surely influence the NH/SH CO emissions (Patra et al., Science, 2014). On the global scale the CO budget might not be influenced too much by the OH field, but given the importance of OH as CO sink, some analysis and discussion about this issue is also needed.

As shown in the updated Fig. 10 above, for the time series of regional annual emissions we now present both the posterior using TransCom and posterior using INCA OH field. Indeed, the distribution of OH field has a considerable impact on the regional budgets. TransCom OH has lower concentration in the NH compared to INCA, thus the inverted emissions using TransCom OH in the NH are generally lower compared to the one using INCA. On the contrary, in the SH where TransCom OH concentration is higher than INCA, the inverted emissions using TransCom OH generates higher CO emissions than INCA. The differences of the two posterior using contrasting OH fields are of a smaller magnitude than the

differences between the posterior and the prior. It is noted that the trends in the posterior emissions are very consistent, irrespective of the OH fields used as shown in the figure below (updated Fig. 9).

Fig. 9. Trend distributions of CO surface emissions from 2002 to 2011 (a) in the prior, (b) in the posterior with TransCom-OH and (c) in the posterior with INCA-OH.



Minor issues:

14507, 23: TES is probably not referring to the “Technology Experiment Satellite”, but to the Tropospheric Emission Spectrometer.

Thanks for point it out. We have corrected it.

14508, 1: "The interpretation : : ": sentence reads awkward, rewrite.

Done. We have revised it as "Comparing modelled and observed trends is complicated by the common biases of atmospheric chemistry-transport models (CTMs) forced with current emission inventories."

14508, 8: "Understanding this model-data misfit is all the more so challenging that surface emissions and chemical production each account for about a half of the total CO sources" ! "Understanding this model-data misfit is challenging because surface emissions and chemical production each account for about half of the total CO source".

Thanks for the edits. It has been implemented as suggested.

14508, 11: can contribute ! could have contributed

We have made the change.

14508, 20: information piece ! piece of information

We have made the change.

14508, 27: to infer the origin of the observed CO concentration decrease in the past decade ! to infer the most likely origin of the observed CO concentration decrease over the past decade

Thanks. We agree it is more accurate stating it in the way as suggested.

14509, 2: remove "at once"

We have made the change.

14509, 4: "chemically connected to hydrocarbons"? unclear

We have replaced this part of the sentence by "a species that only reacts with OH and therefore informs about it".

14509, 13: "The algorithm has undergone continuous improvements and several reprocessings of the archive have been made (Streets et al., 2013)." The algorithm has undergone continuous improvements and the archive has been reprocessed several times (Streets et al., 2013)" By the way: is the Streets et al reference correct? It is not in the list, like the Cressot (2014) reference. Please check all references!

We have made the change in the text as suggested. Thanks for spotting this mistake in the reference. The corresponding reference should be Deeter *et al.*, 2013. In addition, we have double-checked all the references.

14511, 6: this requires some explanation. If you use a "fixed OH field", it is important in know how this has been obtained, and possibly what was the role of NOx in obtaining these fields.

The description was a bit confusing in the old text and we have edited the sentence. The prior OH field is modeled with full chemistry models with NO_x and many other processes considered. The corresponding references for INCA OH is Folberth *et al.*, 2006; and the one for TransCom is Patra *et al.*, 2011 and references therein. In the optimization process, we optimize OH scale over big regions assimilating MCF, CH₄ and CO, during which the effect of

NOx is not relevant.

14511, 14: pressure weighted concentration? Is that not simply a mixing ratio?

Yes. The text has been simplified following the suggestion.

14511, 17: CH₂O has also direct source from biomass burning (Stravakou et al., ACPD, 2015). How do you account for surface emissions in this procedure?

There are direct CH₂O emissions (as shown in Figure 1) in our model both from biogenic and biomass burning emissions in addition to the CH₂O chemical productions from VOC oxidation. The surface emissions are optimized together with the total quantity VOC emissions that will turn into CH₂O (there is a single scaling factor for both).

14511, 27: as described below

We have added the preposition “as” as suggested.

14512, 18: the Cressot reference is not in the list.

It has been added.

14513, 12: Leeuwen ! van Leeuwen

Thanks for pointing it out. It has been added.

14513, 13/16: m² ! m⁻²

It has been changed.

14513, 23: month? The period is 8 days, right?

For our optimization, the period is 8 days; for the prior emission, we use 8-day resolution when the datasets are available. However, the prior emission datasets do not necessarily have such high temporal resolution, in particular for anthropogenic (fuel combustion) emissions. For biomass burning emissions whose daily emissions are available from GFEDv3.1, we calculate weekly mean emissions from the daily emission data. We assume the temporal variability is larger for biomass burning emissions for both CO and CH₄. But for other emission sectors, monthly mean emissions are used as the prior.

14515, 25: what about observational errors? Probably smaller than model errors, but still good to mention.

In the revised text, we have added the global mean measurement error for all the species. “The global mean measurement error for X_{co} is around 6.4±2.9 ppb, which is approximately 8.2±1.9 % of corresponding X_{co} observations. The measurement errors are set as 3 ppb for CH₄ and 1.2 ppt for MCF if not explicitly provided by the surface observation datasets.”

14515, 26: how is the yearly mean of the synoptical variability defined? DO you apply the same filter as for the 3-sigma filtering?

No. The variability of synoptic variability was calculated upstream.

14517, 8: whatever ! irrespective

This has been changed as suggested.

14518, 8: I suggest to add something like: “when for instance the vertical mixing in the model is too conservative, this could lead to a positive bias at the surface, because the sources are adjusted to fit the satellite data.”

Thanks for the suggestion. This example has been added in the text.

14518, 16: Negative ! A negative

We have made the change.

14519, 1: A logical discussion here would be: what are the trends in the direct prior CO emissions from anthropogenic activities and from biomass burning? I see this discussion later...so please point forward to that discussion.

Section 3 focuses on the concentrations, so the underlying attribution from anthropogenic or biomass burning is not yet discussed.

14519, 2: To compare the trend in columns to trends at the surface, please convert the column in a mean mixing ratio.

It is done in the new version. We have converted all the column data from molec cm⁻² into volume mixing ratio (ppb).

14520, 7: I find this not very convincing. To my eye, for at least some stations, it seems the prior simulation reproduces observed trends better than the posterior simulation. So, why not provide the information in a table? (e.g. average improvement of trend).

The trends are now summarized in the following table (Table 2) with information on both the mean bias and the trends.

Table 2. Summary of CO model-data comparison and trend analysis for MOPITT satellite retrievals, surface station observations and corresponding prior/posterior modelling. Trends for each region (in the unit of ppb yr⁻¹) are the mean values for all the grids whose trends are significant at 95% confidence level. The percentages of significant trends are also given per model grid for positive (+) and negative (-) respectively.

REGIONS	MOPITT		Surface		MOPITT column trends								Surface station trends															
	Prior	Post	Prior	Post	Observation				Prior mod				Posterior mod				Observation				Prior mod				Posterior mod			
	Bias	Bias	Bias	Bias	+		-		+		-		+		-		+		-		+		-		+		-	
	(ppb)				N	Trend	%	%	Trend	%	%	Trend	%	%	N	Trend	%	%	Trend	%	%	Trend	%	%	Trend	%	%	
BONA	-14.1	0.7	-20.8	20.5	210	-0.84	99	-0.46	95	-0.88	99	2	-2.51	100	-1.46	100	-2.96	100										
USA	-16.7	-3.1	-20.4	20.1	108	-0.82	97	-0.41	96	-1.08	100	3	-1.67	67	-1.13	100	-3.30	100										
NHSA	-10.0	-3.0			74	-0.61	84	-0.19	8	53	-0.68	100	0															
SHSA	-14.2	0.2			160	-0.59	58	0.38	41		-0.56	67	0															
NHAF	-15.0	-2.0	-20.0	6.8	211	-0.45	7	55	-0.38	85	-0.73	95	1	-0.90	100	-0.73	100	-1.04	100									
SHAF	-16.5	0.5	-1.5	13.6	96	-0.57	75	0.07	27	11	-0.64	96	1	-0.78	100	0.42	100	-0.48	100									
WSEU	-16.1	0.3	-36.7	18.7	106	-1.00	100	-0.49	100	-1.12	100	6	-2.73	100	-2.05	100	-3.51	100										
ESEU	-16.8	0.4			108	-0.77	100	-0.40	100	-0.93	100	0																
BOAS	-17.3	1.0			227	-0.92	99	-0.51	92	-1.02	99	0																
MIDE	-16.5	-2.9			64	-0.57	100	-0.30	100	-0.88	100	0																
SCAS	-12.0	-0.3			80	-0.65	63	-0.30	4	38	-0.92	100	0															
SEAS	-20.1	-3.6	-30.6	22.6	129	-1.23	97	0.13	19	24	-1.35	99	3	-1.76	100	-1.83	100	-3.78	100									
AUST	-15.5	-1.7	-6.4	15.4	105	-0.62	100	0.17	28		-0.78	100	3	-0.34	67	--		-1.18	67									
INDO	-3.8	0.2			64	-1.20	98	-0.84	28	-1.03	98	0																
OCEAN	-11.9	-0.2	-15.1	9.6	3092	-0.72	96	-0.07	22	25	-0.67	97	27	-1.23	4	89	-1.00	7	59	-1.46	89							

14520, 17: fairly agree ! agree fairly well

We have made the change.

14520, 20: trend ! a trend

We have made the change.

14521, 7: "INCA-OH has higher than TransCom OH concentrations in the NH during summer OH maximum, but lower than TransCOM OH concentrations in the SH Tropic" ! INCA has higher OH concentrations than Transcom in the NH during summer, but lower OH concentrations in the SH Tropics"

We have made the change.

14521, 19: A trend of roughly half a percent per year should have an influence on the CO trend (which are typically 0-2.5 %/year). The sink term read -k.CO.OH and trends in CO and OH should be equally important. In figure 8 the posterior trend in the "sink" (k.OH.CO) is also steeper than the posterior trend in the "source", which indicates some role of OH trends (but indeed rather small).

We have rephrased this part as "Such small trends are considered of very small effect on the CO trends."

14521, 20: considered of minor effect on the CO trends ! to be of minor importance for the CO trends

We have made the change.

14522, 5: Please check all units in the paper. For instance, emission maps now have the label "Tg/year", which misses a unit area. In figure 8, the unit should be Tg CO/months, and the trend should also have a unit.

All units for the emission maps are noted as Tg/year, which indeed will be clarified as Tg/year/grid (2.5 degree×3.75 degree). This is the case for both Fig. 2 and Fig. 9. In Fig. 8, the unit should be specified as Tg CO/year (instead of Tg CO), because we have calculated the yearly sum.

14522, 7: SD? You have only two realizations.

The figure has been updated showing the posterior with both OH fields.

14523, 1: more negative ! steeper negative

We have made the change.

14523, 9: no significant trend in the OH concentrations IS found by the inversion: : .but: when the burden of CO decreases, one would expect OH to go up, because one of the most important sinks goes down. In that respect, the absence of an OH-trend is surprising, and I think your results point to a small positive OH trend.

A small positive trend is noticed for the SH (+0.2% yr⁻¹ with TransCom-OH and +0.7% yr⁻¹ with INCA-OH) and a small negative trend in the SH mid-high latitudes (-0.4% yr⁻¹ in TransCom-OH and -0.3% yr⁻¹ in INCA-OH) (14521, 16–20). However, they are really small. We changed the text slightly to be more conservative.

14523, 14: I think that this argument does not make sense. MCF lives 5 years, so a trend in OH anywhere on the globe would be reflected in the MCF mixing ratios also on remote stations.

The signal could be really small in the remote stations if it is not a change through large scales. Meanwhile, different regions could have contrasting changes, but we optimized over big regions. Moreover, the concentration of MCF has been decreasing and is progressively less informative.

14523, 21: This is also incorrect. The Montzka (2011) study only addresses variability, and not trends, since all data were de-trended.

Thanks for pointing this out. We misunderstood the “interannual variability (IAV)” stated in this paper, taking it as normalized values (not de-trended). This was corrected in the revised paper.

14523, 26: unclear why the positive dots appear over oceans. Legend does not explain this.

The reason is that the values over ocean are really small, while the trends are significant. The information has been added in the figure caption.

14523, 28: “estimated by the prior”?? Do you mean: “in the prior emissions”?

Yes. It has been changed.

14524, 28: changing rate ! growth rate?

We have made the change.

14526, 11: “Such decreasing: : observations”. This is not a conclusion of this paper.

We have deleted this point from the conclusion.

14527, 15: OH: like above, invalid argument.

We have modified this argument as “Assimilating observations of CH₂O and other chemically related species could inform more about regional CO budgets, in particular the chemical sources and sinks, and therefore could further improve the top-down estimation of CO budgets for each region.”

Figure 2: Units Tg per year per unit area (gridbox?)

Yes, it is now specified as TgCO/grid.

Reply to Referee #2

We thank the reviewer's appreciation of our work and the thoughtful comments. We have made corresponding efforts to revise the manuscript. The full review is copied hereafter and our responses are inserted where appropriate.

Anonymous Referee #2

Yin et al. use MOPITT version 6 CO retrievals along with surface measurements of methyl-chloroform and methane to perform an atmospheric inversion over 2002-2011. They then use results from the inversion to analyze trend in CO emissions and burdens globally and regionally.

This paper provides an important contribution to atmospheric composition science and should be published in ACP. The methods used are well thought-out, and the paper is generally well written. I have only minor concerns, presented below.

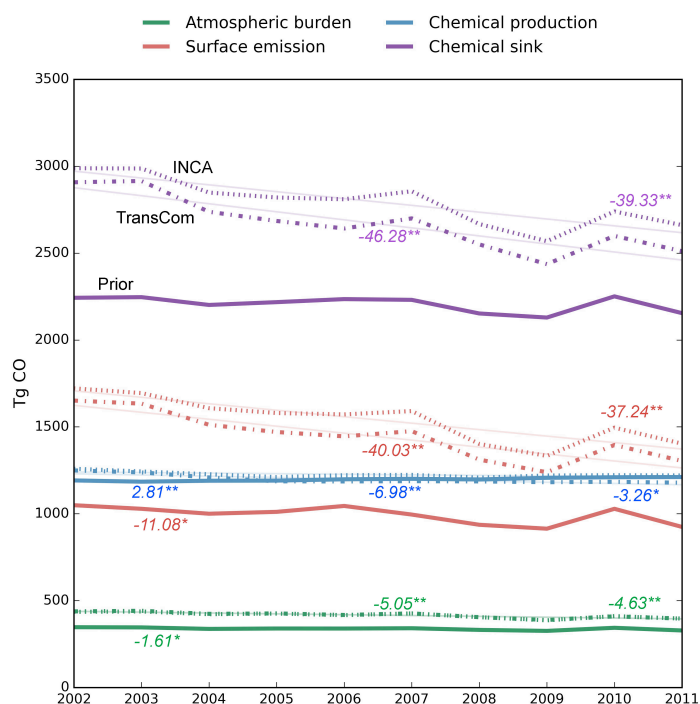
General Comments

1. There are a LOT of numbers in the text, especially in Sect. 3.2 and 5.1. It's very hard to keep track of these and to compare their importance. I think the paper would be well served by including a table with global and regional trends from MOPITT, surface stations and the model sampled like each of these (Sect. 3.2) and another that gives the modeled changes to budget terms (Sect. 5.1). Also, it would be nice to add prior emission (& chemical source/sink) trends to Table 1, since these are perhaps more relevant than the mean amounts and provide context.

Thanks for the suggestion. The text was indeed a bit heavy, we have revised Sect. 3.2 in two ways: adding one table (Table 2, in page 11) to summarize the trends in different regions, and changing the unit for MOPITT retrievals from molec/cm² into mole fractions with numbers more friendly. The entire paragraph is revised accordingly.

For the budgets (Set. 5.1), we updated both Fig. 8 (inserted below) for the global budgets and Fig. 10 (on page 6) for regional emissions in a way that the trends in the prior and posterior are more clearly denoted when the trends are statistically significant. These two revised figures are inserted below.

Fig. 8. Time series of global mean annual CO budget changes from 2002 to 2011. Each component is shown in a different colour. Solid lines indicate the prior (mean values of the two OH fields are shown for the prior chemical CO production and sink). Dash-dot lines represent posterior with TransCom-OH and dotted lines represent posterior with INCA-OH. If the trend is statistically significant, a linear slope is denoted beside each line. With the order from left to right, the numbers represent slopes for the prior, the posterior with TransCom-OH and the posterior with INCA-OH successively. * denotes significant at 95% confidence level, and ** denotes significant at 99% confidence level.



2. There is a large discussion around regional trends, but many of the trends discussed in the text are not in fact significant according to the figures (some are highlighted in the next section). This needs to be made clearer in the text, and I would suggest spending more time on the trends that are in fact significant. For example, one region that is not really discussed but appears interesting is AUST: the prior suggests no trend, but the posterior suggests a very strong negative trend. AUST is referenced briefly in the section on BB, but from comparing Figs. 2b and 9, it looks like the trend is partly driven by locations where BB doesn't dominate. More discussion would be worthwhile.

This confusion carries through to the figures. For example, Fig. 10 includes a lot of trend lines for trends that are highly insignificant, and these are misleading. I would suggest that Figs. 8 and 10 should only show trend lines when the trends are significant. It may also be worth highlighting these by e.g. making the s & p values bold for significant trends, or adding an asterisk. Another option is to put all the values in a table, including their significance, and only include on the figure slopes where the trend is significant.

We thank the reviewer for pointing this out. We have revised this issue in two aspects. First, we have re-run the entire assimilation using improved segmentation methods. In the previous version, in order to save computational time, we did split the period into segments of 14 months with a 2-month overlap between adjacent years. We thought that this approach would not influence the inverted flux trends under the assumption that the initial conditions for each segment are properly optimized by the system with just 2 months of overlap, a spin-up time that is about the lifetime of CO in the atmosphere. Under closer scrutiny, it appears that this segmentation actually generates a small discontinuity in the concentration time series that affects some regional signals. Therefore, we have re-run the inversion with only three segments and with an overlap of 4 months between adjacent segments with initial conditions optimized upstream. The main conclusions are not affected, but all figures will be updated. Some regional trends are slightly changed as shown in Fig. 9 (in page 7).

Second, we have improved the notation of regression slope and significance for Fig. 8 (in page 15) and Fig. 10 (in page 6) as shown above. The discussions about trends are more focused on the significant ones according to the updated results. The negative trend in the posterior emission in SEAS is in fact significant, and we added discussion on the trends in AUST, which is probably explained by the change in burned area as indicated by the newly released GFED4s dataset.

3. Most of the figures are not colorblind-friendly. Figures 3, 4, 6, 7, 8 and 9 all use red and green to contrast two different simulations, which many people cannot interpret (see e.g. <http://www.somersault1824.com/tips-for-designing-scientific-figures-for-color-blind-readers/>). An easy solution would be to change all use of green in these figures to blue.

Thanks very much for this reminder. We have updated all the figures systematically with color schemes of red and blue.

Specific Comments (page, line)

14506, 24-28: This discussion centers around one of the insignificant trends; given this I'm not sure it belongs in the abstract (at least not without explicitly stating that it is insignificant).

In the previous version, China was mentioned particularly in the abstract (for which the trend was significant), but the regional emission was shown for the entire SEAS in Fig. 10, which was a bit misleading. Nevertheless, in the revised results, in which the trends are more robust with the improved segmentation method, the trends in SEAS are indeed significant, so are the trends cover China as shown in Fig. 9. Therefore, we are actually discussing a significant trend.

14507, 22-25: Warner et al. 2013 (doi:10.5194/acp-13-12469-2013) also evaluated CO trends from satellite, and should be cited here.

Thanks for mentioning this study. In the previous version, we cited only the Worden et al. 2013 paper, which synthesized 4 satellite retrievals, and was therefore considered representative of recent trends in satellite observations. The Warner et al. 2013 paper has been added in the revised paper.

14511, 14-18: I am confused by the treatment of CH₂O here. What happens to surface emissions of CH₂O? Are these included in the CH₂O production term? Please clarify.

There are direct CH₂O emissions (as shown in Figure 1) in our model both from biogenic and biomass burning emissions in addition to the CH₂O chemical productions from VOC oxidation. The surface emissions are optimized together with the total quantity VOC emissions that will turn into CH₂O (there is a single scaling factor for both). We have added this description in the paper.

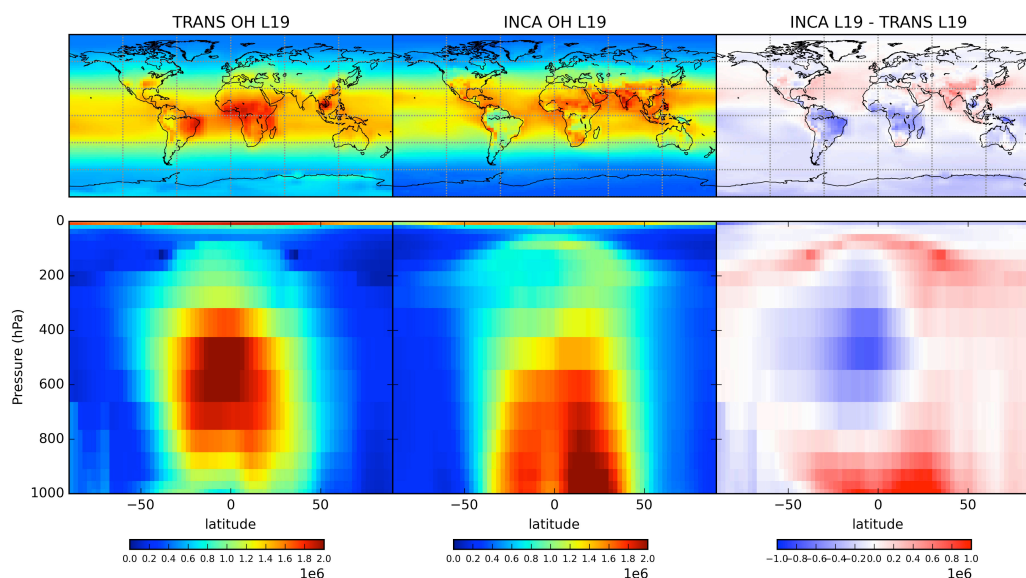
14511, 18-23: I would like to see more justification for splitting OH longitudinally only in the NH. I would expect the active biogenic VOC chemistry in the SH (e.g. the Amazon) to have a large impact on OH that is not longitudinally homogeneous. Is this split neglected because of a lack of SH data constraints, or for some other reason?

Yes, further splitting of the other three latitudinal bands is limited by the number of surface stations. We have added this information in the text.

14512-14513: It would be nice to see a figure showing both OH fields to clarify this discussion. Altitude-latitude zonal mean cross sections would be ideal.

We have added one figure showing both OH fields as well as differences between the two. Fig. 3 in the new version is inserted below.

Fig. 3. Spatial and vertical distribution of OH concentration in TransCom, INCA and differences between the two. The TransCom OH is interpolated from its original 60 pressure levels into the LMDz 19 eta-pressure levels.



14513, 25-26: Does the uncertainty on CH₂O production also include uncertainty on its emission?

Yes. As stated above for 14511, 14-18, the surface CH₂O emissions and chemical productions of CH₂O from VOC emissions are optimized together. There is a single scaling factor for both, so are the uncertainty statistics.

14513, 26: Where are these “initial concentrations” from?

They are simulated from LMDz-INCA full chemistry model and optimized upstream in the revised version. We have added this information in the text.

14515, 4-7: Are there any references for suggesting that some of these observations “may be of lower quality or more difficult to measure?” It would be nice to back this statement up if possible.

The reference is added. Fortems-Cheiney et al., 2011 has explained the observation selection in details.

14515, 25-28: It’s not clear to me what is meant by “yearly means of synoptic variability” – how was this calculated?

It is calculated as the standard deviation of the residual of the detrended and deseasonalized data. We have added this information in the revised paper.

14516, 6-14: Is this a gridded OMI product? If so, what resolution? Do you use the vertical columns here, and are these provided in the product or calculated from slant columns?

We used the OMI CH₂O gridded data with pixel size between 13×24 km² at nadir and 26×135

km² at the swath edges, providing daily global coverage. We used the vertical columns (provided by the product) without convolution of averaging kernel (not provided by the product). This dataset is available from the following site: <http://disc.sci.gsfc.nasa.gov/Aura/data-holdings/OMI/index.shtml>. We have added those details in the revised version.

14516, 18: Most of the calculated values shown later include error bars, and trends include significance. This would be a good place to explain how those are calculated.

It follows the widely used statistical approach in estimating the uncertainties of the linear regressions slope. Here we used the `stat.linregress` function in the `scipy` package in `python2.7`. We did not give the details in the method section, as it is not some method unique to our study.

14517, 18-21: It would be nice to include a statistical measure of goodness of fit, especially for the CH₄ and MCF which aren't shown and therefore makes me wonder how accurate the claim that they fit "fairly well" is.

Thanks for this suggestion. We have added a table to show the goodness of fit as Table 2 inserted below. The substantial decrease of both the mean bias and root mean squares (RMS) reveals the system ability to draw information from the CH₄ and MCF observations.

Table 2. Fitness of CH₄ and MCF observations assimilated in the inversion.

Region	OH-type	CH ₄ (ppb)				MCF (ppt)			
		Mean bias		RMS		Mean bias		RMS	
		<i>prior</i>	<i>posterior</i>	<i>prior</i>	<i>posterior</i>	<i>prior</i>	<i>posterior</i>	<i>prior</i>	<i>posterior</i>
NH(30-90)	<i>TransCom</i>	20.6	2.4	749.6	22.2	1.02	-0.02	1.14	0.05
	<i>INCA</i>	-21.0	2.5	658.1	20.1	0.44	-0.09	0.28	0.07
NH(0-30)	<i>TransCom</i>	15.8	1.5	452.6	19.1	0.90	-0.20	0.91	0.16
	<i>INCA</i>	-21.1	-0.1	564.9	13.9	0.40	-0.20	0.21	0.11
SH(0-30)	<i>TransCom</i>	10.9	-2.4	222.1	20.1	1.19	0.09	1.61	0.13
	<i>INCA</i>	-14.3	-4.0	264.9	29.5	0.88	0.23	0.94	0.15
SH(30-90)	<i>TransCom</i>	14.4	0.2	308.3	4.7	0.88	-0.24	0.90	0.17
	<i>INCA</i>	-7.9	-0.4	96.6	5.7	0.60	-0.06	0.46	0.07

14518, 3-9: Could there be any influence from different amount of land vs. ocean in NH/SH, and different sensitivities of MOPITT over these surfaces? Warner et al. (2013) discuss hemispheric ocean/land differences in AIRS.

We did not test the sensitivity of MOPITT over land vs. ocean, it is not the main focus of this study and we cannot cover every aspect without diverging too much.

14518, 9: Fisher et al. 2015 (doi:10.5194/acp-15-3217-2015) also discuss problems in simulating CO vertical profiles in CTMs, specifically in the SH, and could be cited here.

Thanks for the suggestion; we have added the reference here in the revised paper.

14518, 27: Are these exceptions significant? It's impossible to tell from the small figure.

We have updated the figures and plot only significant trends as shown above in Fig. 10. If significant, the slopes are denoted beside the linear fit with * indicating confidence level of 95% and ** for 99%.

14519, 5: Again, a statistical measure of fit would be nice – it looks like the inversion gets worse relative to the surface stations, but I think that’s just because there are some non-representative large values that draw the eye.

Thanks for the comments; we have added one table to present some statistics of the fitness as shown in Table 3 on page 2 of this reply. The text has also been revised accordingly.

14520, 16: Surely chemistry would play as much or more of a role than NMVOC emissions for CH₂O. There are some recent publications looking at this in the SH (Fisher et al., doi:10.5194/acp-15-3217-2015; Zeng et al., doi:10.5194/acpd-15-2615-2015).

The production of CH₂O is not our main focus in this study. We used the OMI CH₂O column from 2005-2011 to rule out the possibility of large-scale trends in it. At the same time, we acknowledge that our model does not model the CH₂O column perfectly, and further study assimilation OMI CH₂O column would gain some significant benefits.

14520-14521: It doesn’t make any sense for a trend over East Asia to “cancel out” a trend over the Amazon in a latitudinal mean; these would not be in the same latitude bands. Please rephrase this section.

Thanks for pointing it out. We have rephrased this section as “the latitudinal mean however does not bear a significant trend and is thus considered not strong enough to influence the global CO budget.”

14522, 4-7: Are the lines in the figure the means of the 2 OH simulations? Please clarify in the text and/or figure caption.

We have updated Fig. 8 inserted above on page 3, and in the new version we kept both values for TransCom and INCA OH. The relative differences are also addressed.

14524, 2-6: Boreal trends are not significant in prior or posterior.

Thanks for pointing this out; we have emphasized this point in the text. “the same sign of the trends in CO emissions is mostly kept between the prior and the posterior, however, the trends are not statistically significant.”

14524, 13+: Trends in SEAS are not significant in priori or posterior, and in SCAS they are only significant in prior. The discussion that follows is interesting, and still potentially relevant but this needs to be reframed in the context that the optimized simulation shows virtually no trend (highly insignificant with p=0.5).

As explained in the previous reply, this part has been revised thoroughly. The trends are significant according to the updated assimilation. Associated Figure 10 has also been updated (shown in page 4).

14525, 1: ESEU trend is not significant.

For the sum of ESEU emission, the trend is not significant. However, as shown in the trend distribution, the northern part of ESEU, the positive trends are significant. We have

addressed this information more carefully in the revised text.

14525, 13+: African trends not really significant. It's also potentially worth noting in the following discussion that the posterior seems to overestimate amounts and trends in most of Africa (Figs. 3 & 5).

Thanks for pointing this out. The trends are only significant at some grids in the Sahel region and in parts of the South Africa. For the regional sum, the trends in the SHAF is not significant, but the trends in the NHAf is positive since 2006 onward. We will discuss these trends more carefully in the paper revision.

14526, 17: "global annual emission" – is this the mean over all years?

It means the global emission in a certain year.

14526, 22: and South America, from Fig. 9!

This part has been added.

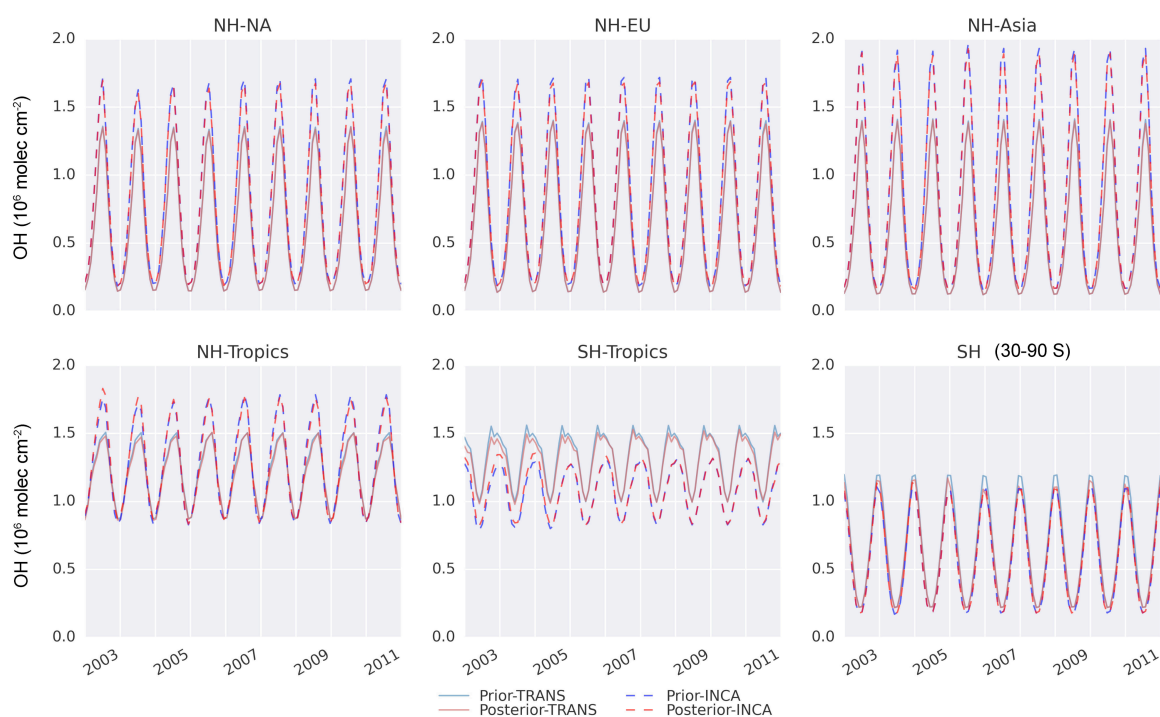
Fig. 6: Which shading is model & which is observations?

The shadings are overlaying and the color differentiation is not so clear. Therefore, we have removed the shading to represent spatial variation in the revised version.

Fig. 7: The change in color scheme for this figure is very confusing. Stick with the same as before (colors show posterior vs. prior, line style shows different OH).

Thanks. We have updated the Fig.7 as suggested here. Use color to show posterior vs. prior and line styles to show different OH.

Fig. 7. Regional volume-weighted monthly mean OH concentrations in the prior and posterior. The results are shown for the 6 big regions in which OH is optimized.



Technical corrections

14508, 6: change “a wrong” to “an incorrect”

Done.

14508, 8: change “more so challenging that” to “more challenging in that”

Done.

14508, 9: change “about a half” to “about half”

Done.

14515, 23: reference to Sect. 2.3.2 must be wrong because this is Sect. 2.3.2, but I’m not sure what section this should be.

Thanks for spotting this. We have revised the consistency in the structure of the manuscript.

14520, 10: change Section 4.1 heading from “concentrations” to “columns”

Done.

14524, 6: change “so are” to “as are”

Done.

14525, 17: change “so are” to “as are”

Done.

Table 1: reference for ocean emissions is different here than the one in the text

It is changed, the Belattaf reference was a French master thesis, we removed it as it is not publicly accessible.

Fig. 4: can you add “n=XX” to each plot to show the number of surface stations averaged in each band?

We have removed this figure, as its content is now summarized in Table 3.

Fig. 5: plots in (a) are too small to see the significance marks; this might work better as 2 columns x 3 rows rather than the way it is now.

We have removed the lower panel to present the distribution of CO.

Fig. 7: “SH (>30S)” is confusing. I suggest “SH (30-90S)”. Fig. 8: add units for the trend values (on figure or in caption). Fig. 10: change “Fig. S1” to “Fig. A1” in caption.

Done.

Decadal trends in global CO emissions as seen by MOPITT

Yi Yin¹, Frédéric Chevallier¹, Philippe Ciais¹, Grégoire Broquet¹, Audrey Fortems-Cheiney²,
Isabelle Pison¹, Marielle Saunois¹

5

¹Laboratoire des Sciences du Climat et de l'Environnement, CEA-CNRS-UVSQ, UMR8212,
Gif-sur-Yvette, France

²[Laboratoire Interuniversitaire des Systèmes Atmosphériques, CNRS/INSU, UMR7583,
Université Paris-Est Créteil et Université Paris Diderot, Institut Pierre Simon Laplace, Créteil,
France](#),

10

Deleted: Institut National de
l'Environnement Industriel et des Risques
(INERIS), Verneuil-en-Halatte, France

Abstract

Negative trends of carbon monoxide (CO) concentrations are observed in the recent decade
15 by both surface measurements and satellite retrievals over many regions of the globe, but
they are not well explained by current emission inventories. Here, we attribute the observed
CO concentration decline with an atmospheric inversion that simultaneously optimizes the
two main CO sources (surface emissions and atmospheric hydrocarbon oxidations) and the
main CO sink (atmospheric hydroxyl radical OH oxidation) by assimilating observations of
20 CO and of chemically related tracers. Satellite CO column retrievals from Measurements of
Pollution in the Troposphere (MOPITT), version 6, and surface observations of methane and
methyl-chloroform mole fractions are assimilated jointly for the period covering 2002-2011.
Compared to the ~~model simulation prescribed with prior emission inventories~~, trends in the
optimized CO concentrations show better agreement with ~~that of~~ independent surface in-situ

Deleted: prior

Deleted: the

30 measurements. At the global scale, the atmospheric inversion primarily interprets the CO
concentration decline as a decrease in the CO emissions ($-2.3\% \text{ yr}^{-1}$), more than twice the
negative trend estimated by the prior emission inventories ($-1.0\% \text{ yr}^{-1}$). The spatial
distribution of the inferred decrease of CO emissions indicates contributions from West
35 Europe ($-4.0\% \text{ yr}^{-1}$), United States ($-4.6\% \text{ yr}^{-1}$) and East Asia ($-1.2\% \text{ yr}^{-1}$) where
anthropogenic fuel combustion generally dominates the overall CO emissions, and also from
Australia ($-5.3\% \text{ yr}^{-1}$), the Indo-China Peninsula ($-5.6\% \text{ yr}^{-1}$), Indonesia ($-6.7\% \text{ yr}^{-1}$), and
South America ($-3\% \text{ yr}^{-1}$) where CO emissions are mostly due to biomass burning. In
contradiction with the bottom-up inventories that report an increase of $2\% \text{ yr}^{-1}$ over China
during the study period, a significant emission decrease of $1.1\% \text{ yr}^{-1}$ is inferred by the
40 inversion. A large decrease in CO emission factors due to technology improvements would
outweigh the increase of carbon fuel combustions and may explain this decrease. Independent
satellite formaldehyde (CH_2O) column retrievals confirm the absence of large-scale trends in
the atmospheric source of CO. However, the CH_2O retrievals are not assimilated and OH
concentrations are optimized at very large scale in this study. Future studies could investigate
45 potential sub-regional trends in the atmospheric sources of CO or in the OH concentrations,
and thus further refine the estimation of regional CO emissions and associated trends.

Deleted: in terms of both distributions and trends

Deleted: , and finds noticeable trends neither in the chemical oxidation sources of CO, nor in the OH concentrations that regulate CO sinks. The latitudinal comparison of the model state with independent formaldehyde (CH_2O) columns retrieved from the Ozone Measurement Instrument (OMI) confirms the absence of large-scale trends in the atmospheric source of CO. The global CO emission decreased by 17% during the decade

Deleted: both a decrease in fossil- and bio-fuel emissions over

Deleted: the USA

Deleted: a decrease in biomass burning emissions in

Deleted: , Indonesia, Australia and Boreal regions

Deleted: An emission decrease of $2\% \text{ yr}^{-1}$ is inferred in China,

Deleted: one of the main emitting regions, in

Deleted: e

Deleted: observed

Deleted: In Africa, instead of the negative trend ($1\% \text{ yr}^{-1}$) reported by CO emission inventories mainly contributed by biomass burning, a positive trend ($1.5\% \text{ yr}^{-1}$) is found by the atmospheric inversion, suggesting different trends between satellite-detected burned areas and CO emissions.

1 Introduction

80 Carbon monoxide (CO) is an air pollutant that leads to the formation of tropospheric ozone (O₃) and carbon dioxide (CO₂) (Jacob, 1999). It is the major sink of the tropospheric oxidant hydroxyl radical (OH), and hence influences concentrations of methane (CH₄) and non-methane volatile organic compounds (NMVOCs) (Logan *et al.*, 1981). It contributes to an indirect positive radiative forcing of 0.23±0.07 Wm⁻² at the global scale (Stocker *et al.*,
85 2013). Atmospheric CO has two main sources: (i) direct surface CO emissions from fuel combustion and biomass burning, estimated to be ~500-600 TgCO yr⁻¹ and ~300-600 TgCO yr⁻¹, respectively, by emission inventories (Granier *et al.*, 2011 and references herein), and (ii) secondary chemical oxidation of hydrocarbons in the troposphere, estimated to be a source of ~1200-1650 TgCO yr⁻¹ with considerable differences among studies (Holloway *et al.*, 2000; Pétron *et al.*, 2004; Shindell *et al.*, 2006; Duncan and Logan, 2008). The sink of
90 CO is mainly through oxidation by OH (Logan *et al.*, 1981), which defines an average lifetime of 2 months for CO in the atmosphere.

Surface in-situ measurements in Europe (Zellweger *et al.*, 2009; Angelbratt *et al.*, 2011), over the USA (Novelli *et al.*, 2003; EPA, 2011), in some large cities in China (Li and Liu, 2011),
95 and in many other places (Yoon and Pozzer, 2014) indicate that CO concentrations have been decreasing for more than ten years. Negative trends have also been observed by various satellite sensors (MOPITT, [Tropospheric Emission Spectrometer](#) - TES, and Atmospheric
Infrared Sounder - AIRS) over most of the world (Warner *et al.*, 2013; Worden *et al.*, 2013). In particular, strong CO concentration decreases are seen from these satellite retrievals over
100 East China and India (Worden *et al.*, 2013), where bottom-up inventories report increasing emissions (Granier *et al.*, 2011; Kurokawa *et al.*, 2013).

Deleted: Technology Experiment Satellite

Atmospheric chemistry-transport models (ACTMs) prescribed with emission inventories are commonly used to analyze the role of emissions on the atmospheric concentration. Most of

105 these simulations tend to underestimate CO concentrations in the mid to high latitudes of the northern hemisphere (NH), whereas they overestimate them over emission hotspots (Shindell *et al.*, 2006; Duncan *et al.*, 2007; Naik *et al.*, 2013; Stein *et al.*, 2014; Yoon and Pozzer, 2014). This bias reveals an incorrect balance between CO sources, at the surface and in the atmosphere, and CO sinks (Naik *et al.*, 2013). Understanding this model-data misfit is

110 challenging because surface emissions and chemical production each account for about half of the total CO sources, and because the sink term removes an amount of CO equivalent to all the sources within a few weeks. Changes in each source and sink term could have contributed to the observed CO concentration decrease, even though only CO emission trends are usually discussed (Khalil and Rasmussen, 1988; Novelli *et al.*, 2003; Duncan and Logan, 2008).

115 In principle, the attribution of the mean balance between sources and sinks and of their trends can be made with Bayesian inversion systems that infer the CO budget terms based on (i) measurements of CO and species related to the CO sources and sinks, (ii) some prior information about the budget terms and spatial distributions, (iii) a CTM model to link emissions and chemistry to concentrations, and (iv) a description of the uncertainty in each

120 piece of information. Various inversion studies have estimated regional or global CO budgets using CO surface observations (Bergamaschi *et al.*, 2000; Pétron, 2002; Butler *et al.*, 2005) or satellites retrievals (Arellano *et al.*, 2004; Pétron *et al.*, 2004; Stavrou and Müller, 2006; Chevallier *et al.*, 2009; Fortems-Cheiney *et al.*, 2009, 2011, 2012; Kopacz *et al.*, 2010; Hooghiemstra *et al.*, 2012a; Jiang *et al.*, 2013). Here, we use the inversion system Python

125 Variational – Simplified Atmospheric Chemistry (PYVAR-SACS) of Pison *et al.* (2009), Chevallier *et al.* (2009) and Fortems-Cheiney *et al.* (2009, 2011, 2012) to infer the most likely origin of the observed CO concentration decrease over the past decade (2002-2011).

Deleted: The interpretation of trend differences or similarities between models and observations is made complicated by the fact that most atmospheric chemistry-transport models (CTMs) forced with current emission inventories

Deleted: wrong

Deleted: all the more so

Deleted: that

Deleted: a

Deleted: that

Deleted: an

Deleted: piece

In contrast to most CO inversion systems cited above, which focused on a single species, PYVAR-SACS simultaneously assimilates observations of the main species in the chemical oxidation chain of CH₄-CH₂O-CO and methyl chloroform (MCF), a species that only reacts with OH and therefore informs about its concentration. The PYVAR-SACS system optimizes the interconnected sources and sinks of the four species in a statistically and physically consistent way at the model resolution of 3.75°×2.5° (longitude, latitude) on an 8-day basis, therefore being suitable for addressing the above-described attribution problem of the CO variations within the limit of the observation information content.

Deleted: at once

Deleted: is chemically connected to hydrocarbons through its only reaction with OH

The primary data source about CO in this study is MOPITT, a multi-channel thermal infrared (TIR) and near infrared (NIR) instrument on board the EOS-Terra satellite (Deeter, 2003). MOPITT provides the longest consistent time series of satellite CO retrievals to date. The algorithm has undergone continuous improvements and the archive has been reprocessed several times (Deeter *et al.*, 2013). Most of the above-cited satellite-based inversion studies used version 4 or earlier versions of the MOPITT CO retrievals, in which a noticeable instrumental drift was reported (Deeter *et al.*, 2010). In version 5, this drift has been corrected together with other improvements (Deeter *et al.*, 2013; Worden *et al.*, 2013). Here, we use the further improved version 6, that has no noticeable bias in the trends of the CO total column (Deeter *et al.*, 2014), to attribute the CO concentration decline by assimilation in our atmospheric inversion system.

Deleted: several

Deleted: -

Deleted: ings of the archive have been made

Deleted: Streets *et al.*, 2013

The structure of the paper is as follows. Section 2 describes the inversion system and the datasets. Section 3 presents the inversion results on CO concentrations and associated trends. We show a brief evaluation of the inversion ability to fit the assimilated data and we cross evaluate the optimized surface CO concentrations against independent station measurements. Then, we compare the CO concentration trend in the MOPITT retrievals, in the surface measurements, and in corresponding modelling results before and after the inversion. Section

4 shows the trend analysis of the prior and the posterior simulated CH₂O and OH
175 concentrations. CH₂O concentrations are representative of the chemical CO sources and we
evaluate the model values against retrievals of its dry air column ($X_{\text{CH}_2\text{O}}$) made from
observations of Ozone Monitoring Instrument (OMI) aboard EOS Aura. OH regulates CO
sinks, but is an extremely short-lived compound whose concentrations are difficult to
measure (Mao *et al.*, 2012). Lacking direct global observation data, we discuss its
180 uncertainties with two contrasting prior OH fields. Section 5 presents the inverted CO budget,
including atmospheric burden, emission, chemical production and chemical loss. Section 6
summarizes this work, discusses the sources of uncertainties and provides some perspectives
for future works.

185 2 Method and data

2.1 Inversion system

The PYVAR Bayesian inversion system, initially introduced by Chevallier *et al.* (2005), aims
at adjusting a series of target variables (jointly called \mathbf{x}), so that they become consistent with
both the atmospheric observations (\mathbf{y}) and a priori state (\mathbf{x}^b) given their respective
190 uncertainties, represented by error covariance matrices \mathbf{R} and \mathbf{B} . By iteratively minimizing
the following cost function J , PYVAR finds the optimal solution for \mathbf{x} in a statistical sense:

$$J(\mathbf{x}) = \frac{1}{2}(\mathbf{x} - \mathbf{x}^b)^T \mathbf{B}^{-1}(\mathbf{x} - \mathbf{x}^b) + \frac{1}{2}(\mathbf{H}(\mathbf{x}) - \mathbf{y})^T \mathbf{R}^{-1}(\mathbf{H}(\mathbf{x}) - \mathbf{y})$$

where \mathbf{H} is the combination of a CTM and of an interpolation operator that includes the
combination with the retrieval prior CO profiles and averaging kernels (AKs) for MOPITT.

195 Our CTM is the general circulation model of Laboratoire de Météorologie Dynamique (LMDz) version 4 (Hourdin *et al.*, 2006), nudged towards winds analysed by the European Centre for Medium-Range Weather Forecasts, run in an off-line mode with precomputed atmospheric mass fluxes, and coupled with the chemistry module SACS (Pison *et al.*, 2009). SACS is a simplification of the full chemistry model Interaction with Chemistry and Aerosols (INCA, Hauglustaine, 2004).

The chemical chain is shown in Fig. 1. It includes surface emissions of CO, CH₄, CH₂O and MCF. The 3D contribution of NMVOCs oxidation to CH₂O production has been pre-calculated by the full chemistry transport model LMDz-INCA (Folberth *et al.*, 2006). OH links all the species together. Reaction kinetic and photolysis rates, as well as fields of species that are not represented as tracers in PYVAR-SACS (e.g. O₁D, O₂, Cl) are based on the LMDz-INCA simulation. The initial states are produced by LMDz-INCA. The CTM in PYVAR-SACS has a time step of 15 minutes for the dynamics (advection) and of 30 minutes for the physics (convection, boundary layer turbulence) and chemistry, a horizontal resolution of 3.75°×2.5° (longitude, latitude), and a vertical resolution of 19 eta-pressure levels from the surface to the top of the atmosphere.

The state vector **x** contains the following variables as shown in the grey boxes in Fig. 1: (1) grid-point scaling factors for the initial mixing ratios of the four trace gas species (CO, CH₄, CH₂O, MCF); (2) grid-point 8-day mean surface emissions of CO, CH₄, and MCF; (3) grid-point 8-day scaling factors to adjust the sum of CH₂O surface emissions and CH₂O production from NMVOC oxidation; (4) 8-day scaling factors to adjust the column-mean OH concentrations over 6 big boxes of the atmosphere over the globe: 3 latitudinal boxes (90°S-30°S, 30°S-0°, 0°-30°N) and 3 longitudinal boxes north of 30°N (North America: 180°W-45°W, Europe: 45°W-60°E, Asia: 60°E-180°E). The longitudinal division of the band north of 30°N is an improvement compared to previous PYVAR studies with 4 latitudinal bands in

Deleted: , and the effects of NO_x are not considered

Deleted: pressure-weighted column-mean concentrations

Deleted: pressure-weighted column-mean atmospheric

Deleted: s

Deleted: pressure-weighted

Deleted: U

Deleted: (

230 total to optimize OH. As there are available surface stations with long-term MCF
235 observations within each of the sub-regions, thus allows adjusting separately continental
differences of OH.

Deleted:)

Deleted: as it should

2.2 A priori information

Previous configurations of PYVAR-SACS have been described by [Chevallier et al. \(2009\)](#)
235 and [Fortems-Cheiney et al. \(2011\)](#). We have improved the configuration as described below.

2.2.1 Prior sources and sinks

For prior anthropogenic fossil fuel and biofuel CO emissions, we use the monthly MACCity
emission inventory of [Lamarque et al. \(2010\)](#) that arguably underestimates emissions less
than other global inventories ([Granier et al., 2011](#); [Stein et al. 2014](#)). For biomass burning,
240 we updated the version of Global Fire Emissions (GFED) from [version 2 \(van der Werf et al.,
2006\)](#) to [version 3.1 \(Van der Werf et al., 2010\)](#). The latter has various improvements
including the definition of different fire types, with specific consideration for deforestation
and peatland fires. [We also increased the temporal resolution of biomass burning emissions
from monthly to weekly \(aggregated from GFEDv3.1 daily emissions, Mu et al., 2011\).](#)
245 Additionally, we consider in this study biochemical CO emissions from oceans, that were
neglected before, based on an ocean biogeochemical model simulation ([Aumont and Bopp,
2006](#)). These monthly ocean CO fluxes add up to a global annual sum of 54 TgCO yr⁻¹
without inter-annual variability. We still consider neither biogenic CO emissions over land,
nor surface CO deposition, because these two terms are relatively small and are of a similar
250 order of magnitude ([Duncan et al., 2007](#)). The prior CO emissions are summarised in Table 1
and the distribution of the mean annual prior CO surface emissions is shown in Fig. 2a. The
relative contribution of biomass burning is shown in Fig. 2b.

255 The prior CH₄ and MCF emissions have also been updated compared to Fortems-Cheiney *et al.* (2012) and are similar to that of Cressot *et al.*, (2014). 3D HCHO production prior fields have been pre-calculated by LMDz-INCA (Folberth *et al.*, 2006), with prescribed NMVOC emission datasets detailed in Fortems-Cheiney *et al.* (2012). The prior distribution of mean annual CO chemical sources in the troposphere from the oxidation of both CH₄ and
260 NMVOCs are shown vertically integrated in Fig. 2c.

Previous PYVAR-SACS studies used prior OH information from a multi-year simulation by LMDz-INCA (Hauglustaine, 2004). Here, we use another field that was prepared for the international TransCom-CH₄ experiment of Patra *et al.*, (2011). The annual mean horizontal and vertical distribution of OH concentrations for both OH fields and their differences are shown in Fig. 3. Compared to the INCA-OH, the TransCom OH has a lower OH concentration in the NH, and a lower concentration over the Tropics and SH. Thus the
265 TransCom-OH has a north-south inter-hemisphere ratio around 1, whereas the INCA-OH has a ratio of 1.2. There are also vertical differences between these two OH-fields: in general, TransCom-OH has higher OH concentrations in the mid-troposphere over the Tropics and in
270 the top layers above 100 hPa, whereas INCA-OH has higher OH concentrations in the lower troposphere below 700 hPa. The prior distribution of the CO sinks simulated with TransCom-OH is shown vertically integrated in Fig. 2d.

2.2.2 Prior error statistics

The prior flux uncertainty, defined by the standard deviation (SD) of each grid-point 8-day
275 flux, is described below. For CO emission uncertainties, we define the SD for each year based on the maximum value of the emission time series during the corresponding year for each grid point (noted as f_{\max}), in order to account for the uncertainty of the fire timing. Then, to account for (i) the possibility of undetected small fires that can contribute to as much as

Deleted: We call this field

Deleted: . It

Deleted: of

Deleted: considerably

Deleted: s

Deleted: over

Deleted: slightly

Deleted: 8

Deleted: prescribed

35% of the global biomass burning carbon emissions (Randerson *et al.*, 2012), and (ii) potentially higher CO emission factors during small fires that were not specifically considered in current fire emission inventories (van Leeuwen *et al.*, 2013), we define a fire emission threshold of $1.0 \cdot 10^{-10} \text{ kg CO}_2 \text{ m}^{-2} \text{ s}^{-1}$. If the prior emission is less than the threshold (no fire a priori, but there could be one in reality), the SD is set as 100% of f_{max} ; otherwise (fire a priori, but possibly of a too small magnitude), the SD is set as the maximum value between $1.0 \cdot 10^{-9} \text{ kg CO}_2 \text{ m}^{-2} \text{ s}^{-1}$ and 50% of f_{max} . In such a way, we allow the system to relax the constraint on the prior emission to account for undetected small emissions, but we keep the global uncertainty ($\sim 180 \text{ TgCO}_2 \text{ yr}^{-1}$) consistent with current bottom-up inventories (Granier *et al.*, 2011; Van der Werf *et al.*, 2010). For simplicity, this error setting also serves for anthropogenic fuel consumption.

The prior CH₄ emission uncertainty is defined as 100% of the maximum value of the prior emissions in the grid cell and its eight neighbours in the corresponding month. The MCF prior emission uncertainty is set at $\pm 10\%$ of the flux, as its emissions are supposed to be well known. The uncertainty of CH₂O production is assumed to be 100% of its concurrent prior CH₂O production. The uncertainties of initial concentration scaling factors are set at 10% for the four species (CO, CH₄, CH₂O, MCF). Errors on OH 8-day scaling factors are set at $\pm 10\%$. The spatial error correlations of the a priori are assigned to all variables following Chevallier *et al.* (2007), defined by an e-folding length of 500 km over the land and 1000 km over the ocean. Temporal error correlations are defined by an e-folding length of 8 weeks for MCF and 2 weeks for the other species including OH. No inter-species flux error correlations are considered.

310 2.3 Observations for assimilation

Deleted: /

Deleted: /

Deleted: /

Deleted: /

315 **2.3.1 Datasets**

We assimilate three data streams: (i) MOPITTv6 satellite CO total column retrievals (noted as X_{CO} hereafter) and surface in-situ measurements of (ii) CH₄ and (iii) MCF.

MOPITT retrievals are available since March 2000, but the instrument experienced a cooler failure from May 2001 to August 2001, which artificially changed the retrieval mean level
320 (Deeter *et al.*, 2010). An instrument anomaly also led to a 2-month lack of data in 2009 from the end of July until September, without any significant change in the retrieval mean level. For the sake of consistency, given our focus on trends, we select the measurements for the decade from 2002 to 2011, during which both the MOPITT retrievals and the prior emission inventories are homogeneous (GFEDv3.1 has not been publicly updated for the years after
325 2011).

We use the level 2 “multispectral” near and thermal infrared (NIR/TIR) CO retrievals of MOPITTv6 that offer the best description of CO in the lower troposphere among the MOPITT products (Deeter *et al.*, 2014). The MOPITT vertical profiles (prior and retrieved CO profiles and associated AKs) are defined on ten vertical pressure levels. Given the limited
330 vertical resolution of the retrievals and the focus on surface emissions, it has been common practice in previous inversion studies starting from Pétron *et al.* (2004) to assimilate the 700-hPa pressure level retrievals only, as a good compromise between proximity to the surface and limited noise. However, Deeter *et al.* (2014) noted that the retrievals at some individual vertical levels still suffered from small bias drifts while such drifts were not seen in the
335 retrieved integrated columns. Furthermore, the interpretation of vertically-integrated columns in the inversion is less hampered by flaws in CTM vertical mixing and vertical sink distribution than for level retrievals (Rayner and O’Brien, 2001). For these two reasons, we assimilate the column retrievals rather than level retrievals. Night-time observations,

Deleted: X_{CO} (with their original prior CO profiles and AKs)

observations with solar zenith angle larger than 70 degrees, with latitudes within 25 degrees from the poles, or with surface pressures less than 900 hPa are excluded, since they may be of lower quality or more difficult to model (Fortems-Cheiney *et al.*, 2011). We average the

22×22 km² retrievals at the 3.75°×2.5° model resolution within 30-minute time steps. The model X_{CO} retrievals are calculated in a consistent way as in the MOPITT X_{CO} retrievals with their original prior CO profiles and AKs averaged for each model grid.

Surface measurements of CH₄ and MCF from various networks are assimilated together with MOPITT X_{CO}. The datasets are downloaded from the World Data Centre for Greenhouse Gases (WDCGG, <http://ds.data.jma.go.jp/gmd/wdcgg/>). Stations that recorded more than 6 years of data without gaps larger than 1 year are included. The list of stations is given in Tables S1 and S2. For the surface measurements, a data filtering process is conducted in order to remove outliers that the global model may not be able to capture. We exclude (i) observations exceeding 3σ of the de-trended and de-seasonalized daily time series and (ii) observations whose misfit against the prior simulation exceeds 3σ of the de-trended and de-seasonalized misfit between observations and forward modelling values.

2.3.2 Observation error statistics

The observation error covariance matrix **R** is diagonal in order to simplify calculations. Observation errors are combinations of measurement errors (quantified by the data providers), representativeness errors and CTM errors. For X_{CO}, as we have averaged a large amount of observations in each grid-box (see Section 2.3.1), the representativeness error is effectively much reduced and is not considered specifically. The CTM error is set at 30% (SD) of the modelled values for X_{CO}. For CH₄ and MCF, synoptic variability (estimated from the residues of de-trended and de-seasonalized data) is used as a proxy for the CTM and representativeness errors, which largely dominate the observation error. The global mean

Field Code Changed

Deleted: 2

Deleted: the yearly means of

measurement error for Xco is around 6.4±2.9 ppb, which is approximately 8.2±1.9 % of corresponding Xco observations. The measurement errors are set as 3 ppb for CH4 and 1.2 ppt for MCF if not explicitly provided by the surface observation datasets.

370 **2.4 Observations for cross evaluation**

We use two datasets for independent evaluation of the inversion results.

The first one is made of CO surface observations archived at the WDCGG. The same site selection and data filtering process as for CH₄ and MCF surface measurements are applied (see the list of stations in Table S3).

375 The second evaluation dataset gathers CH₂O total columns retrieved from OMI by the Smithsonian Astrophysical Observatory (SAO). We use version 3, release 2, of this product (González Abad *et al.*, 2015). Since this data is not available before mid-2004, it does not cover our study period completely: for the sake of consistency, we do not assimilate it (in contrast to Fortems-Cheiney *et al.* 2012) and we keep it for evaluation. We select
380 observations that are tagged as “good” by the provider’s quality flag, which have a solar zenith angle less than 70 degrees, a cloud cover below 20%, and are not affected by the “row anomaly”.

2.5 Trend analysis

The long-term trend in this study is estimated by least-square curve fitting of the following
385 function, which includes a constant, a linear component, and seasonal variations represented by four harmonics:

$$f(t) = a_0 + a_1 t + \sum_{n=1}^4 c_n [\sin(2n\pi t + \varphi_n)]$$

If not particularly specified, all the trends mentioned in this paper refer to a_1 .

390 3 CO concentrations and associated trends

3.1 Evaluation of the inversion framework's ability to fit the data

395 Fig. 4a shows the time series of global mean mole fraction of the MOPITT X_{CO} retrievals (black), the prior (blue) and the posterior (red) X_{CO} retrievals (calculated from model simulations with the MOPITT prior profiles and averaging kernels). Compared to the MOPITT X_{CO} , the prior X_{CO} simulation is on average 15% lower when modelled with TransCom-OH and 17% lower when modelled with INCA-OH. The global mean posterior X_{CO} fits the observation irrespective of the OH field used.

400 The spatial distribution of the multiyear mean X_{CO} observed by MOPITT (2002-2011) shows a latitudinal gradient from north to south, with some high values over East Asia, Africa and central South America (Fig. 4b). The regional mean bias of X_{CO} in the prior and the posterior modelling compared to the MOPITT data are summarized in Table 2. The prior simulation is generally lower than the observations except in parts of Indonesia and India (Fig. 4c). This negative bias agrees with previous studies (Arellano *et al.*, 2004; Fortems-Cheiney *et al.*, 2011; Hooghiemstra *et al.*, 2012a, Naik *et al.*, 2013; Shindell *et al.*, 2006), and thus calls attention to understanding and correcting it appropriately (Stein *et al.*, 2014). The optimized CO concentrations fit the measurements quite well (Fig. 4d), illustrating the inversion's ability to fit the data.

410 Similarly for CH_4 and MCF, Table 3 summarizes the mean biases and residual root mean squares (RMS) of the prior and posterior modelling values compared to the station observations that are assimilated in the system over four latitudinal bands. The inversion fits

- Deleted: The
- Deleted: X_{CO} from
- Deleted: observations
- Deleted: is shown for the period from Sep. 2001 to Oct. 2014 in Fig. 3a, and
- Deleted: green
- Deleted: assimilations
- Deleted: are shown for the period from 2002 to 2011, with four months in 2001 for spin up
- Deleted: concentrations
- Deleted: whatever
- Deleted: Fig. 3b presents t
- Deleted: map
- Deleted: . It
- Deleted: $(2.14 \pm 0.19 \cdot 10^{18} \text{ molec cm}^{-2})$ between 30-60°N
- Deleted: $(1.16 \pm 0.09 \cdot 10^{18} \text{ molec cm}^{-2})$ between 30-60°S
- Deleted: $(2.5 \pm 0.4 \cdot 10^{18} \text{ molec cm}^{-2})$
- Deleted: $(1.95 \pm 0.3 \cdot 10^{18} \text{ molec cm}^{-2})$
- Deleted: $(1.8 \pm 0.1 \cdot 10^{18} \text{ molec cm}^{-2})$
- Deleted: 3
- Deleted: $(-0.24 \pm 0.1 \cdot 10^{18} \text{ molec cm}^{-2})$
- Deleted: 3
- Deleted: better
- Deleted: 3
- Deleted: t

the assimilated data fairly well, with a considerable decrease in both the mean biases and the RMS (Table 3).

The mean biases of the prior and posterior simulations compared to independent surface in-situ CO measurements are also summarized for each region in Table 2. For the oceanic background stations (over 27 model grid cells), the magnitude of the model-data misfits decreased considerably after inversion. Over land, the changes in model-data misfit after inversion are more heterogeneous. The prior bias is in general negative, whereas the sign changed from negative to positive for the posterior. The magnitude of the posterior bias (also the RMS, not shown in the table) decreased significantly in West Europe (WSEU), South East Asia (SEAS) and North Hemisphere Africa (NHAF), and they are of similar magnitudes in Boreal North America (BONA) and the USA. However, the mean bias and RMSs increased in South Hemisphere Africa (SHAF) and Australia (AUST).

This seemingly deterioration of the modelled surface concentrations could be explained by several reasons: First, surface station measurements and model grids (2.5x3.75 degree) have different spatial representativeness. In fact, at most background oceanic stations, the model-data misfit suggests an overall improvement after inversion. Second, the vertical sensitivities are different between satellite column retrievals and surface observations (Hooghiemstra *et al.*, 2012). Over regions where fire emission injection heights are sometimes above the boundary layer (Cammis *et al.*, 2009) or where chemical CO sources in the mid-troposphere contributes significantly to the CO column (Fisher *et al.*, 2015), the surface CO concentrations are less influenced by these sources, but the model may not capture this vertical distribution of sources. Third, there might be a model bias in modelling the vertical CO profiles in the CTM (Jiang *et al.*, 2013), for instance, when the vertical mixing in the model is too conservative, it could lead to a positive bias at the surface, because the sources are adjusted to fit the satellite data. Nevertheless, such discrepancies between X_{CO} column

- Deleted: ,
- Deleted: but these results are not shown, as they are not the main focus in this study
- Deleted: Compared
- Deleted: the
- Deleted: , the optimized CO concentrations better fit the observations in terms of both mean values and trends
- Deleted: (Fig
- Deleted: .
- Deleted: 4)
- Deleted: magnitude of the model-data misfits after optimization is considerably reduced compared to the prior model-data misfits. The magnitude of posterior misfits is decreased by 61% (19.4 ppb) in the NH - North of 30N (Fig. 4a), by 72% (12.7 ppb) in the NH-Tropics (Fig. 4b) and by 62% (9.2 ppb) in the SH-Tropics (Fig. 4c). The posterior misfit in the Southern Hemisphere (SH) - South of 30S is of a similar magnitude (7.3 ppb) to the prior misfit (-7.7 ppb), but the sign changed from negative to positive (Fig. 4d). While the prior model-data misfits are mostly negative, the posterior misfits generally show small positive signs, especially over the SH
- Deleted: ly
- Deleted: the total column sensitivity of satellite retrievals may not inform well enough
- Deleted: as seen by surface observations
- Deleted: and secondly
- Deleted: of
- Deleted: .

and surface concentration do not seem to bear a significant trend. For instance, significant trends in the prior misfits were found in the NH (0.67 ± 0.24 ppb yr⁻¹), NH-Tropics (0.77 ± 0.16 ppb yr⁻¹) and SH-Tropics (-0.42 ± 0.14 ppb yr⁻¹), and they are corrected in the posterior misfits to non-significant after assimilation.

3.2 Distribution of trends in CO concentrations

The spatial distributions of trends in the MOPITT X_{CO} and in the prior and the posterior X_{CO} over the period from 2002 to 2011 are shown successively in Fig. 5. Regional mean trends in both the X_{CO} and surface CO concentrations are summarized in Table 2.

MOPITT X_{CO} retrievals show negative trends in most regions of the world except for the Sahel region in Africa and some areas of central South America and India (Fig. 5a). In the MOPITT retrievals, the negative trends are particularly large over Indonesia (-1.20 ppb yr⁻¹), South East Asia (-1.23 ppb yr⁻¹) and the Northern Pacific and Atlantic Ocean (-1.15 ppb yr⁻¹). The global average trend in the MOPITT X_{CO} is -0.67 ppb yr⁻¹, accounting for a decrease of around 0.91% yr⁻¹ over the globe, and the trends in the prior and posterior X_{CO} retrievals are -0.12 ppb yr⁻¹ (-0.28% yr⁻¹) and -0.70 ppb yr⁻¹ (-0.93% yr⁻¹) respectively. The spatial correlations between the trends of the MOPITT X_{CO} and the prior/posterior X_{CO} are 0.55 and 0.81 respectively, showing considerable improvements after inversion.

In general, negative trends in the prior X_{CO} are underestimated (Fig. 5b and Table 2), and positive trends are simulated over Southeast Asia (19%), South Hemisphere South America (41%), South Africa (27%), Australia (28%), with percentages of model grid cells that have significant positive trends noted in the brackets. In addition, 22% of the oceanic grid cells are modelled with positive trends in the prior simulation, but none is noticed in the MOPITT

- Deleted: - ... [3]
- Deleted: positive
- Deleted: present
- Deleted:
- Deleted: and
- Deleted: 66
- Deleted: 4
- Deleted: changed
- Deleted: smaller negative trends of -0.48 ± 0.15 ppb yr⁻¹ in the NH and
- Deleted: in the NH-Tropics
- Deleted: (Fig. 4a and b)
- Deleted: . Such trends in the posterior misfits are within the uncertainty ranges of the trends in the observations (-2.5 ± 0.6 ppb yr⁻¹ in the NH and -1.1 ± 0.4 ppb yr⁻¹ in the NH-Tropics). Negative trend in the prior misfit of -0.42 ± 0.14 ppb yr⁻¹ is seen in the SH-Tropics where no significant trend is found in the latitudinal mean concentration, and the trends in prior misfits are corrected after assimilation (Fig. 4c).
- Deleted: in
- Deleted: CO concentrations
- Deleted: from
- Deleted: is
- Deleted: The upper row successively shows ... [4]
- Deleted: The global average trend is ... [5]
- Deleted: The
- Deleted: $3.0 \pm 1.1 \cdot 10^{16}$ molec cm⁻²
- Deleted: $2.5 \pm 0.9 \cdot 10^{16}$ molec cm⁻²
- Deleted: $2.6 \pm 0.3 \cdot 10^{16}$ molec cm⁻²

column retrievals (Deeter *et al.*, 2014). Trends in the posterior X_{CO} generally agree with the MOPITT X_{CO} and the positive trends in the prior X_{CO} are corrected (Fig. 5c and Table 2).

Surface in-situ measurements also show a general negative trend in CO concentration (Table 2). The negative trends from in-situ CO stations have the largest magnitude in the NH mid-latitudes over West Europe (-2.7 ± 1.7 ppb yr^{-1}) and the USA (-1.6 ± 0.9 ppb yr^{-1}). Smaller trends are found in the SH in-situ sites (-0.32 ± 0.14 ppb yr^{-1}). The trends over Asia indicate large spatial heterogeneity (-1.6 ± 1.3 ppb yr^{-1}) and the trends over the Tropics show a small but insignificant increase (0.3 ± 1.6 ppb yr^{-1}), but these regions are represented by a limited number of stations.

Compared to these surface in-situ measurements, the prior simulation generally tends to underestimate the magnitude of the negative ones, and the posterior slightly overestimate them. The global mean trends are -1.3 ppb yr^{-1} (-1.1% yr^{-1}) in the observation, -0.87 ppb yr^{-1} (-0.75% yr^{-1}) in the prior simulations, and -1.9 ppb yr^{-1} (-1.2% yr^{-1}) in the posterior simulations. However, it is noted that the global mean trends are only represented by 72 stations that are not evenly distributed over the globe. Positive trends in the prior simulated surface CO are less visible compared to the total column as shown in Fig 5b and Table 2. It could be explained by the respective vertical weighting of these two observation types, but the difference may also be enhanced by changes in the MOPITT AKs if the retrieval prior is biased (Yoon *et al.*, 2013). However, this comparison is limited by the representativeness of a few sites.

4 Concentrations of CH₂O and OH

4.1 CH₂O columns

Field Code Changed

Deleted: In general, the s

Deleted: stations

Deleted: present

Deleted: trends

Deleted: Fig. 5d

Deleted: s

Deleted: 9

Deleted: that are sparsely distributed

Deleted: -

<#>In the posterior simulation (sampled the (sampled the same way as the prior simulation with the MOPITT AKs), a general decreasing trend appears with the same distribution as in the assimilated satellite observations (compare Fig. 5c and 5a). When the posterior simulation is sampled at the surface stations, which were not used in the inversion (Fig. 5f), most locations show similar negative trends as the trends in observations. As described in section 3.1 (Fig. 4), the discrepancies in the trends between our prior simulation and the observations at the surface stations are corrected in our posterior simulation. -

Deleted: more

Deleted: pronounced than those of the prior simulated surface CO (Fig. 5e), given

Deleted: stations in these two regions are relatively sparse and may not be representative for regional trends compared to satellite retrieval trends

Deleted: <#>In the posterior simulation (sampled the same way as the prior simulation ... [6]

Deleted: concentrations

The mean time series of CH₂O total columns for four latitudinal zones are shown in Fig. 6. X_{CH₂O} retrievals were not assimilated (contrary to the CH₄ and MCF surface measurements that affect the sources and sinks of CH₂O in the inversion), and the inversion actually does not change X_{CH₂O} much. This suggests that the differences between simulated and satellite-retrieved X_{CH₂O} are mainly caused by the prior NMVOC emissions used in the full chemistry run of LMDz-INCA. The latitudinal mean values of prior/posterior modelled X_{CH₂O} agree fairly well with the OMI retrievals without any obvious bias, but the seasonal cycle is different especially in the Northern mid-high latitudes both in phase and in amplitude (Fig. 6a). The OMI X_{CH₂O} retrievals, the prior and the posterior simulations all agree about the absence of a significant trend in the latitudinal average of X_{CH₂O} for the period from 2005 to 2011, which is consistent with the hypothesis that the equilibrium between the oxidation of hydrocarbons into CH₂O and the sink of CH₂O into CO has not significantly changed, at least at continental scales. We note that the OMI X_{CH₂O} retrievals describe some trends at smaller scales, like positive trends of 3±0.8 % yr⁻¹ over East Asia (De Smedt *et al.*, 2010) and negative trends of -1.9±0.6 % yr⁻¹ over the Amazon, but they are not significant for the mean values of large latitudinal bands, and are thus considered not large enough to influence the global CO budget.

Deleted: fairly

Deleted: cancel each out on the

Deleted: means

670 4.2 OH concentrations

Fig. 7 shows the latitudinal average of the prior (blue) and posterior (red) OH concentrations for the 6 big regions over which OH is optimized (see Section 2.1). This figure reports the two inversions that use either TransCom-OH (solid lines) or INCA-OH (dashed lines; see Section 2.2.1). INCA has higher OH concentrations than TransCom in the NH in particular

Deleted: prescribed

Deleted: dashed lines

Deleted: optimized

Deleted: solid lines

Deleted: in red

Deleted: in green

Deleted: -OH

Deleted: than TransCom

during summer, but lower OH concentrations in the SH Tropics all year long and slightly lower concentrations in the SH mid-high latitudes (South of 30S) during summer peaks.

Deleted: OH maximum

Deleted: than TransCOM

In general, larger corrections are applied by the inversion to INCA-OH than to TransCom-OH. The inversion system adjusts the INCA-OH concentrations towards TransCom-OH by downscaling the OH concentrations in the NH during summers, especially over Asia, where INCA-OH is considerably higher than the TransCom-OH (Fig. 3). A small reduction of the TransCom-OH concentrations is also seen in the SH.

Deleted: 7

The two inversions do not produce significant trends in OH during the study period for most regions, except for a very small positive trend in the SH Tropics (+0.2% yr⁻¹ with TransCom-OH and +0.7% yr⁻¹ with INCA-OH) and a small negative trend in the SH mid-high latitudes (-0.4% yr⁻¹ in TransCom-OH and -0.3% yr⁻¹ in INCA-OH). Such small and insignificant trends are considered to be of minor importance for the CO trends. The OH scaling is addressed more in details in section 5.1 when discussing CO sinks.

Deleted: effect on

5 Optimized sources and sinks of CO

After having documented the prior and the posterior misfits with MOPITTv6 and with cross validation data for the latitudinal mean values and for the trends, which lends support to the consistency of the inversion results with these data-streams, we now turn to the implications for CO sources and sinks.

5.1 Inverted CO budget

The global annual CO atmospheric burden, surface emissions, chemical production, and chemical loss of the prior and the posteriors with the two OH experiments from 2002 to 2011 are shown in Fig. 8. Averaging over the 10 years, a considerable increase of the mean CO

Deleted: The dashed lines present the prior budget and the solid lines the posterior budget in each term; the shaded areas around the solid lines indicate the standard deviation between the two OH experiments.

atmospheric burden (+23%, in dark green) is seen in the posterior compared to the prior simulation. Accordingly, increases of CO emissions (+50%, in red) and chemical sinks with OH (+23%, in purple) are produced in the posterior, whereas only a very small change is noticed for the CO chemical sources (+1%, in blue). The magnitude of the increment in the global CO emissions is larger compared to previous studies that assimilate the 700 hPa retrieval levels of MOPITT using a similar inversion set up (Fortems-Cheiney *et al.*, 2011, 2012). The cross evaluation against surface station measurements also shows a considerable positive bias in the posterior CO concentration (section 3.1), which implies a potential bias in the modelling of vertical CO profiles. Nevertheless, for our study here focusing on trends, such systematic model error do not seem to harm the robustness of the trends as shown in section 3 and 4. The chemical sink of CO is a function of both CO and OH. Given the results for OH adjustments shown in section 4.2 (generally small reduction from the prior OH), the increase of the CO sink in the posterior is thus mainly due to the increase of CO concentrations after assimilation.

The inversion produces a negative trend of around 10% per decade in the global atmospheric burden of CO ($-5.1 \pm 0.9 \text{ TgCO yr}^{-1}$ with TransCom-OH and $-4.6 \pm 0.8 \text{ TgCO yr}^{-1}$ with INCA-OH), which is twice the negative trend of CO atmospheric burden produced by the prior emissions ($-1.6 \pm 0.6 \text{ TgCO yr}^{-1}$, i.e. a decrease of 5% per decade in the simulated CO burden). For CO sources, the trend of prior CO emissions is of $-11.1 \pm 4.4 \text{ TgCO yr}^{-1}$ (equivalent to a decrease of 10% per decade). This is mostly contributed by the negative trend in biomass burning emissions in GFEDv3.1 ($-10.6 \pm 3.7 \text{ TgCO yr}^{-1}$) and by a very small decrease in anthropogenic emissions in MACCity ($-0.68 \pm 0.4 \text{ TgCO yr}^{-1}$) from 2002 to 2011. Compared to the prior emissions, a two-fold steeper negative trend in terms of percentages is found in the posterior CO emissions, 24% per decade with TransCom-OH ($-40 \pm 7.2 \text{ TgCO yr}^{-1}$) and 22% per decade with INCA-OH ($-37 \pm 7.1 \text{ TgCO yr}^{-1}$). A small positive trend ($2.8 \pm 7.1 \text{ TgCO}$

- Deleted: 4
- Deleted: 39
- Deleted: 17
- Deleted: -
- Deleted: 3
- Deleted: The chemical CO source here is calculated from the oxidation of CH₄ and CH₂O (indirectly from NMVOCs), whose concentration fields generally agree with independent observations as shown above in section 4.1.
- Deleted: of $-4.8 \pm 0.8 \text{ TgCO yr}^{-1}$
- Deleted: equivalent to a decrease of 10% per decade
- Deleted: 8
- Deleted: These trends are calculated from the mean results of TransCom-OH and INCA-OH inversions and uncertainties noted here represent the uncertainty of the regression.
- Deleted: 4
- Deleted: 3
- Deleted: 6
- Deleted: 09
- Deleted: more
- Deleted: -26.1
- Deleted: 4
- Deleted: 5
- Deleted: (
- Deleted: 17
- Deleted: The

775 yr^{-1} , equivalent to an increase of 2% per decade) is produced in the prior CO chemical production, mostly contributed by the increase of methane oxidation. The posterior CO chemical production shows a small negative trend. Yet, as CH_2O concentrations are not constrained by observations, this small trend may result from the system's inability to differentiate the two CO sources between surface emissions and chemical oxidations.

780 For the CO sink, a larger trend in the posterior ($-46.3 \pm 8.3 \text{ TgCO yr}^{-1}$, 16% per decade with TransCom-OH and $-39.3 \pm 8.0 \text{ TgCO yr}^{-1}$, 13% per decade with INCA-OH) is found, while there is no significant trend in the prior chemical sink. This negative trend in the posterior is mostly due to the decrease of CO concentrations in the atmosphere that change the amount of CO oxidized by OH , and only very small trends in the OH concentrations are found by the inversion. Such small trends are considered of very small effect on the CO trends. The OH concentrations are optimized for 6 big regions over the globe and the MCF concentrations are

785 monitored at background sites only, which allows a coarse zonal estimate of OH but leaves spatially heterogeneous land areas unconstrained, e.g. polluted areas near cities (Hofzumahaus *et al.*, 2009), forests with high NMVOC emissions (Lelieveld *et al.*, 2008) or biomass burning plumes (Folkins *et al.*, 1997; Rohrer *et al.*, 2014). Therefore, sub-regional trends in OH, if they exist, are not necessarily captured in this study. In addition, with the

790 exponential decrease of MCF concentrations in recent years (only a few parts per trillion, ppt, at the current level), the constraining strength of MCF on OH in the inversion system may not be even from 2002 to 2011, even though the same sites and a similar number of observations were assimilated. Nevertheless, the zonal trend of OH should still be constrained throughout most of the period and previous studies suggest that the inter-annual change of global OH

795 concentration is within 5% (Montzka *et al.*, 2011).

- Deleted: s
- Deleted: both
- Deleted: and t
- Deleted: s
- Deleted: are small and not statistically significant
- Deleted: 28
- Deleted: 9
- Deleted: 5
- Deleted: 10
- Deleted: compared to the prior simulation ($-11.0 \pm 3.6 \text{ TgCO yr}^{-1}$, 4.8% per decade)
- Deleted: at each time step
- Deleted: no significant trend
- Deleted: Yet,
- Deleted: t
- Deleted: observation

Deleted: and bears no significant trend for the period from 1998 to 2007

5.2 Regional distribution of trends in CO emissions

The distributions of trends in CO emissions after optimization are very consistent using either TransCom-OH or INCA-OH (Fig. 9); therefore, only trends of TransCom-OH experiments are discussed here. The relative contribution of biomass burning to the total land surface emissions estimated in the prior emission is shown in Fig. 2b. The time series of the prior and the two posterior annual CO emissions using two different OH fields are shown for each sub-region in Fig. 10. The division in sub-regions is illustrated in Fig. A1. As shown in Fig. 10, the choice of prior OH concentrations could potentially have a large impact on the regional CO emission estimates; nevertheless, the inverted emission trends are quite robust and we do not discuss further in this paper the regional emission increments and the sensitivities of inverted fluxes to prior OH or chemical CO productions.

For the boreal regions where CO emissions are mainly due to biomass burning (Boreal Asia - BOAS and Boreal North America - BONA), the same sign of the trends in CO emissions is mostly kept between the prior and the posterior, but the amplitude of the trends are updated into larger values, as are the emission amounts. It should be noted that MOPITT CO retrievals over high latitudes beyond 65° are not included in the assimilation.

For the NH mid-latitudes where CO emissions are mainly due to fossil fuel and biofuel burning emissions (USA, West Europe - WSEU, East Europe - ESEU, Middle East - MIDE, South Central Asia - SCAS, South East Asia - SEAS), consistencies between the trends in the prior and the posterior CO emissions are found in the developed countries (Fig. 9). For example in the USA and WSEU regions, decreasing trends produced by the emission inventories generally agree with the atmospheric signals (Lamarque *et al.*, 2010). On the contrary, the inversion changes the sign of the CO trend over SEAS (including China) and SCAS (including India), where the prior emissions suggested a significant increase.

Consistent with our posterior emissions, a gradual decrease of CO emissions in China after the year 2005 was actually deduced from CH₄/CO₂ and CO/CO₂ correlations observed off the

Deleted: results

Deleted: of the assimilation using

Deleted: The distributions of trends in the prior and the posterior CO emissions over the globe are shown in Fig. 9.

Deleted: by

Deleted: for each sub-region

Deleted: and t

Deleted: S

Deleted: o

Deleted: n

coast of East Asia from 1999-2010 (Tohjima *et al.*, 2014). A decrease of the emission factors of other co-emitted species of CO during fossil fuel or biofuel combustion has also been noted: for instance, a decrease of black carbon emission factors in China and India was reported by Wang *et al.* (2014), and a decrease in the relative ratio of NO_x to CO₂ from 2003 to 2011 was observed from satellite retrievals over East Asia (Reuter *et al.*, 2014). These studies and our results suggest that combustion technology improvements in East Asia resulted in emission factor reduction to an extent that outweighs the impact of increasing fossil fuel burning. In this scenario, emission inventories would well report the latter but not the former that is more difficult to quantify. In addition, trends of fossil fuel emissions are updated (Lamarque *et al.*, 2010) but not trends of biofuel burning, especially for traditional biofuels (Yevich and Logan, 2003). A small difference in the trend of CO emissions in East Europe (ESEU) is also noticed (not significant though), an emission peak in the year 2010 is inferred from the inversion.

865 For the tropical and sub-tropical regions, where CO emissions are mainly attributed to biomass burning, the inversion does not change the sign of trends over Indonesia (INDO). The positive trends of the prior emissions over the Indo-China Peninsula (2% yr⁻¹) are updated into negative ones (-5.6% yr⁻¹) by the inversion. Negative trends over Australia except for the central area (on average -5.3% yr⁻¹), and over SHSA (-3% yr⁻¹, but not significant for the regional mean) are largely enhanced compared to the prior trends (Fig. 9). The spatial distribution of this negative trend is consistent with the new version of GFEDv4 burned area (not used in this study) (Giglio *et al.*, 2013), which accounts for small fires that were not explicitly included in GFEDv3.1 used here as the prior. In Australia, the decrease of CO emissions might be explained by decreased fire emissions (Poulter *et al.*, 2014). The decrease in SHSA could be attributed to a decrease of deforestation fires in recent years,

Deleted: changing rate

Deleted: with much

Deleted: higher

Deleted: s

Deleted: than estimated in the prior

Deleted: contributed by

Deleted: in most regions of Southern Hemisphere South America (SHSA),

Deleted: and Australia (AUST), though the amplitude of the trends changes (Fig. 9). For instance, the inversion produces larger negative trends over SHSA than the prior. A significant decreasing trend in SHSA is observed in the burned area, in agreement with the new version of GFEDv4 burned area

Deleted: This

Deleted:

especially after 2005 (Meyfroidt and Lambin, 2011), although there are uncertainties in the overall deforestation rates (Kim *et al.*, 2015).

895 The change in trends between the prior and the posterior CO emissions is more heterogeneous over Africa (Northern Hemisphere Africa - NHAF and Southern Hemisphere Africa - SHAF). Decreases in the burned area have been observed over the NHAF Sahel region, as are decreases in the prior CO emissions, which are explained by changes in both precipitation and the conversion of savannah into cropland (Andela and van der Werf, 2014).

900 But positive trends in CO emissions are inferred by the atmospheric inversion especially since 2006, except for some small areas. The different signs of the trend in burned area (or the prior CO emissions) and the posterior CO emissions may be explained by the change in CO emission factors that could vary a lot with the conversion of fire type from savannah fire to agricultural burning and also with precipitation change (van Leeuwen *et al.*, 2013). In addition, increases of anthropogenic fossil fuel and biofuel emission in the NHAF region could also contribute to some of the differences (Al-mulali and Binti Che Sab, 2012). Differences between the prior and the posterior CO emissions are also noticed for the central part of the SHAF. The increase in the GFED4 burned area is explained by the increase of precipitation that allows more fuel accumulation, as driven by the El Niño/Southern Oscillation (ENSO) changes from El Niño to La Niña dominance over the recent decade (Andela and van der Werf, 2014). The opposite negative trend of CO emissions in the posterior could be explained by a decrease in CO emission factors when the fuel load and combustion completeness are high so that less carbon is emitted in the form of CO; but the dynamics of emission factors are not modelled in the bottom-up estimation (van Leeuwen *et al.*, 2013). In addition, small fires that are not considered in our prior biomass emissions could also contribute to such differences (Randerson *et al.*, 2012).

905

910

915

Deleted: large

Deleted: so

Deleted: On the contrary in our study,

Deleted: a

Deleted: region

Deleted: in Cameroon.

6 Conclusion

925 CO concentrations observed by both MOPITTv6 satellite X_{CO} retrievals and surface in-situ measurements show significant negative trends over most of the world from 2002 to 2011.

The CO concentration trends in the forward CTM simulations prescribed with CO emission inventories show considerable inconsistency with the observed MOPITT X_{CO} from 2002 to 2011. By assimilating MOPITTv6 X_{CO} and surface measurements of CH_4 and MCF, the

930 inversion system suggests that the decrease in the atmospheric CO concentrations is mainly

attributable to a decrease of 23% in surface emissions during the study period at the global scale. The trends in the prior and the posterior CO emissions agree well with each other over the USA and Western Europe. The largest differences between the prior and the posterior CO

emission trends are noticed for South East Asia, Australia and parts of South America and

935 Africa. Decreases of CO emissions are found in Central China, while the prior emission

inventories suggest increases. This emission decrease is probably caused by a large decrease of emission factors due to technology improvements that outweigh the increase of emission

activities. CO emissions from biomass burning decreased considerably in Indonesia and

Australia. For Africa, the contrasts of trends between the prior and the posterior likely reflect

940 different trends between satellite-detected burned area and CO emissions due to changes in

combustion completeness, CO emission factors, and the relative contribution of small fires.

The amplitude of the trends also differs in many other regions, illustrating the original information brought by atmospheric inversions about CO emissions.

No significant trend is found in the latitudinal-mean OH concentrations, and a sensitivity test

945 made with two different OH fields suggests consistent results in the OH trend. It is however

noted that we optimized OH over six big-regions globally, and sub-regional trends in the OH

concentrations, if they exist, are not accounted for in this study. We also acknowledge the

Deleted: Such decreasing trends have continued until the end of 2014 according to the latest MOPITT observations.

Deleted: 17

Deleted: The inverted global annual emission has decreased from 1506 TgCO yr⁻¹ to 1235 TgCO yr⁻¹, when simulated with our reference OH field (TransCom-OH).

Deleted: parts of

Deleted: and India

Deleted: s

Deleted: large changes

Deleted: in the trends

Deleted: s

Deleted: because we optimize it in six big regions only

limited information content of MCF to constrain OH in recent years over the study period.

965 For chemical CH₂O production from NMVOC oxidation, the system has the potential to generate regional increments, but CH₂O is not assimilated here due to limited temporal coverage of the OMI data from 2005 to 2011. Assimilating observations of CH₂O and other chemically connected species could inform more about regional CO budgets, in particular the chemical sources and sinks, and therefore could further improve the top-down estimation of
970 CO budgets for each region in future studies.

Deleted: No noticeable trend for this period is observed in the latitudinal mean CH₂O concentrations, which are representative of the equilibrium between the oxidation of hydrocarbons into CH₂O and the sink of CH₂O into CO. It is however noted that some small regional trends in X_{CH₂O} are missed by the inversion. These unconstrained sub-regional trends in OH and CH₂O suggest a

Deleted: from

Deleted: to increase the constraints on

Deleted: each term

Deleted: the

985 Acknowledgements

The authors acknowledge the support of the French Agence Nationale de la Recherche (ANR) under grant ANR-10-BLAN-0611 (project TropFire). F.C. is funded by the European Commission under the EU H2020 Programme (grant agreement No. 630080, MACC III). The
990 NCAR MOPITT and the SAO OMI retrievals are available from <https://www2.acd.ucar.edu/mopitt> and http://disc.sci.gsfc.nasa.gov/Aura/data-holdings/OMI/omhcho_v003.shtml, respectively. We thank both institutes for having brought this data into open access and thank Dr. González Abad for helpful information about the OMI product. Similarly, we also acknowledge the WDCGG for providing the archives of
995 surface station observations for MCF, CH₄ and CO. We thank the following persons who have participated to the surface in-situ measurements through various networks: NOAA (E. Dlugokencky, G.S. Dutton, J.W. Elkins, S.A. Montzka, P.C. Novelli), CSIRO (P.B. Krummel, R.L. Langenfelds, L.P. Steele), EC (D. Worthy), Empa (B. Buchmann, M. Steinbacher, L. Emmenegger), JMA (Y. Fukuyama), LSCE (M. Ramonet), NIWA (G.
1000 Brailsford, S. Nichol, R. Spoor), UBA (K. Uhse), UNIURB (J. Arduini), and AGAGE (P.J. Fraser, C.M. Harth, P.B. Krummel, S. O'Doherty, R. Prinn, S. Reimann, L.P. Steele, M. Vollmer, R. Wang, R. Weiss, D. Young). Finally, we wish to thank F. Marabelle and his team for computer support at LSCE.

1005

References

- Al-mulali, U. and Binti Che Sab, C. N.: The impact of energy consumption and CO₂ emission on the economic growth and financial development in the Sub Saharan African countries, *Energy*, 39(1), 180–186, doi:10.1016/j.energy.2012.01.032, 2012.
- Angelbratt, J., Mellqvist, J., Simpson, D., Jonson, J. E., Blumenstock, T., Borsdorff, T., Duchatelet, P., Forster, F., Hase, F., Mahieu, E., De Mazière, M., Notholt, J., Petersen, A. K., Raffalski, U., Servais, C., Sussmann, R., Warneke, T. and Vigouroux, C.: Carbon monoxide (CO) and ethane (C₂H₆) trends from ground-based solar FTIR measurements at six European stations, comparison and sensitivity analysis with the EMEP model, *Atmos. Chem. Phys.*, 11(17), 9253–9269, doi:10.5194/acp-11-9253-2011, 2011.
- Arellano, A. F., Kasibhatla, P. S., Giglio, L., van der Werf, G. R. and Randerson, J. T.: Top-down estimates of global CO sources using MOPITT measurements, *Geophys. Res. Lett.*, 31(1), L01104, doi:10.1029/2003GL018609, 2004.
- Aumont, O. and Bopp, L.: Globalizing results from ocean in situ iron fertilization studies, *Global Biogeochem. Cycles*, 20(2), GB2017, doi:10.1029/2005GB002591, 2006.
- Belattaf, A.: Modélisation des sources océaniques de CO et d'isoprène, Master Thesis U. Versailles Saint-Quentin, 32pp, 2012.
- Bergamaschi, P., Hein, R., Heimann, M. and Crutzen, P. J.: Inverse modeling of the global CO cycle: 1. Inversion of CO mixing ratios, *J. Geophys. Res.*, 105(D2), 1909, doi:10.1029/1999JD900818, 2000.
- Butler, T. M., Rayner, P. J., Simmonds, I. and Lawrence, M. G.: Simultaneous mass balance inverse modeling of methane and carbon monoxide, *J. Geophys. Res.*, 110(D21), D21310, doi:10.1029/2005JD006071, 2005.
- Cammas, J.-P., Brioude, J., Chaboureau, J.-P., Duron, J., Mari, C., Mascart, P., Nédélec, P., Smit, H., Pätz, H.-W., Volz-Thomas, A., Stohl, A. and Fromm, M.: Injection in the lower stratosphere of biomass fire emissions followed by long-range transport: a MOZAIC case study, *Atmos. Chem. Phys.*, 9(15), 5829–5846, doi:10.5194/acp-9-5829-2009, 2009.
- Chevallier, F., Bréon, F.-M. and Rayner, P. J.: Contribution of the Orbiting Carbon Observatory to the estimation of CO₂ sources and sinks: Theoretical study in a variational data assimilation framework, *J. Geophys. Res.*, 112(D9), D09307, doi:10.1029/2006JD007375, 2007.
- Chevallier, F., Fisher, M., Peylin, P., Serrar, S., Bousquet, P., Bréon, F. M., Chédin, A. and Ciais, P.: Inferring CO₂ sources and sinks from satellite observations: Method and application to TOVS data, *J. Geophys. Res.*, 110(D24), 2005.

- Chevallier, F., Fortems, A., Bousquet, P., Pison, I., Szopa, S., Devaux, M. and Hauglustaine, D. A.: African CO emissions between years 2000 and 2006 as estimated from MOPITT observations, *Biogeosciences*, 6(1), 103–111, 2009.
- 1045 Cressot, C., Chevallier, F., Bousquet, P., Crevoisier, C., Dlugokencky, E. J., Fortems-Cheiney, A., Frankenberg, C., Parker, R., Pison, I., Scheepmaker, R. A., Montzka, S. A., Krummel, P. B., Steele, L. P. and Langenfelds, R. L.: On the consistency between global and regional methane emissions inferred from SCIAMACHY, TANSO-FTS, IASI and surface measurements, *Atmos. Chem. Phys.*, 14(2), 577–592, doi:10.5194/acp-14-577-2014, 2014.
- 1050 Deeter, M. N.: Operational carbon monoxide retrieval algorithm and selected results for the MOPITT instrument, *J. Geophys. Res.*, 108(D14), 4399, doi:10.1029/2002JD003186, 2003.
- Deeter, M. N., Edwards, D. P., Gille, J. C., Emmons, L. K., Francis, G., Ho, S. P., Mao, D., Masters, D., Worden, H., Drummond, J. R. and Novelli, P. C.: The MOPITT version 4 CO product: Algorithm enhancements, validation, and long-term stability, *J. Geophys. Res.*, 115(D7), doi:DOI: 10.1029/2009JD013005, 2010.
- 1055 Deeter, M. N., Martínez-Alonso, S., Edwards, D. P., Emmons, L. K., Gille, J. C., Worden, H. M., Pittman, J. V., Daube, B. C. and Wofsy, S. C.: Validation of MOPITT Version 5 thermal-infrared, near-infrared, and multispectral carbon monoxide profile retrievals for 2000–2011, *J. Geophys. Res. Atmos.*, 118(12), 6710–6725, 2013.
- 1060 Deeter, M. N., Martínez-Alonso, S., Edwards, D. P., Emmons, L. K., Gille, J. C., Worden, H. M., Sweeney, C., Pittman, J. V., Daube, B. C. and Wofsy, S. C.: The MOPITT Version 6 product: algorithm enhancements and validation, *Atmos. Meas. Tech. Discuss.*, 7(6), 6113–6139, doi:10.5194/amtd-7-6113-2014, 2014.
- 1065 Duncan, B. N. and Logan, J. A.: Model analysis of the factors regulating the trends and variability of carbon monoxide between 1988 and 1997, *Atmos. Chem. Phys.*, 8(24), 7389–7403, doi:10.5194/acp-8-7389-2008, 2008.
- Duncan, B. N., Logan, J. a., Bey, I., Megretskaia, I. a., Yantosca, R. M., Novelli, P. C., Jones, N. B. and Rinsland, C. P.: Global budget of CO, 1988–1997: Source estimates and validation with a global model, *J. Geophys. Res.*, 112(D22), D22301, doi:10.1029/2007JD008459, 2007.
- 1070 EPA: National Trends in CO Levels, [online] Available from: <http://www.epa.gov/airtrends/carbon.html> (Accessed 12 February 2014), n.d.
- Fisher, J. A., Wilson, S. R., Zeng, G., Williams, J. E., Emmons, L. K., Langenfelds, R. L., Krummel, P. B. and Steele, L. P.: Seasonal changes in the tropospheric carbon monoxide profile over the remote Southern Hemisphere evaluated using multi-model simulations and aircraft observations, *Atmos. Chem. Phys.*, 15(6), 3217–3239, doi:10.5194/acp-15-3217-2015, 2015.
- Folberth, G. A., Hauglustaine, D. A., Lathière, J. and Brocheton, F.: Interactive chemistry in the Laboratoire de Météorologie Dynamique general circulation model: model description and

- impact analysis of biogenic hydrocarbons on tropospheric chemistry, *Atmos. Chem. Phys.*, 6(8), 2273–2319, doi:10.5194/acp-6-2273-2006, 2006.
- 1080 Folkens, I., Wennberg, P. O., Hanisco, T. F., Anderson, J. G. and Salawitch, R. J.: OH, HO₂, and NO in two biomass burning plumes: Sources of HO_x and implications for ozone production, *Geophys. Res. Lett.*, 24(24), 3185–3188, doi:10.1029/97GL03047, 1997.
- 1085 Fortems-Cheiney, A., Chevallier, F., Pison, I., Bousquet, P., Carouge, C., Clerbaux, C., Coheur, P.-F., George, M., Hurtmans, D. and Szopa, S.: On the capability of IASI measurements to inform about CO surface emissions, *Atmos. Chem. Phys.*, 9(22), 8735–8743, 2009.
- 1090 Fortems-Cheiney, A., Chevallier, F., Pison, I., Bousquet, P., Saunois, M., Szopa, S., Cressot, C., Kurosu, T. P., Chance, K. and Fried, A.: The formaldehyde budget as seen by a global-scale multi-constraint and multi-species inversion system, *Atmos. Chem. Phys.*, 12(15), 6699–6721, 2012.
- Fortems-Cheiney, A., Chevallier, F., Pison, I., Bousquet, P., Szopa, S., Deeter, M. N. and Clerbaux, C.: Ten years of CO emissions as seen from Measurements of Pollution in the Troposphere (MOPITT), *J. Geophys. Res.*, 116(D5), doi:DOI: 10.1029/2010JD014416, 2011.
- 1095 Giglio, L., Randerson, J. T. and van der Werf, G. R.: Analysis of daily, monthly, and annual burned area using the fourth-generation global fire emissions database (GFED4), *J. Geophys. Res. Biogeosciences*, 118(1), 317–328, doi:10.1002/jgrg.20042, 2013.
- González Abad, G., Liu, X., Chance, K., Wang, H., Kurosu, T. P. and Suleiman, R.: Updated Smithsonian Astrophysical Observatory Ozone Monitoring Instrument (SAO OMI) formaldehyde retrieval, *Atmos. Meas. Tech.*, 8(1), 19–32, doi:10.5194/amt-8-19-2015, 2015.
- 1100 Granier, C., Bessagnet, B., Bond, T., D'Angiola, A., Denier van der Gon, H., Frost, G. J., Heil, A., Kaiser, J. W., Kinne, S., Klimont, Z., Kloster, S., Lamarque, J.-F., Liousse, C., Masui, T., Meleux, F., Mieville, A., Ohara, T., Raut, J.-C., Riahi, K., Schultz, M. G., Smith, S. J., Thompson, A., Aardenne, J., Werf, G. R. and Vuuren, D. P.: Evolution of anthropogenic and biomass burning emissions of air pollutants at global and regional scales during the 1980–
- 1105 2010 period, *Clim. Change*, 109(1-2), 163–190, doi:10.1007/s10584-011-0154-1, 2011.
- Hauglustaine, D. A.: Interactive chemistry in the Laboratoire de Météorologie Dynamique general circulation model: Description and background tropospheric chemistry evaluation, *J. Geophys. Res.*, 109(D4), D04314, doi:10.1029/2003JD003957, 2004.
- 1110 Hauglustaine, D. A., Granier, C., Brasseur, G. P. and Mégie, G.: The importance of atmospheric chemistry in the calculation of radiative forcing on the climate system, *J. Geophys. Res.*, 99(D1), 1173, doi:10.1029/93JD02987, 1994.
- Hofzumahaus, A., Rohrer, F., Lu, K., Bohn, B., Brauers, T., Chang, C.-C., Fuchs, H., Holland, F., Kita, K., Kondo, Y., Li, X., Lou, S., Shao, M., Zeng, L., Wahner, A. and Zhang, Y.: Amplified trace gas removal in the troposphere., *Science*, 324(5935), 1702–4,

- 1115 doi:10.1126/science.1164566, 2009.
- Holloway, T., Levy, H. and Kasibhatla, P.: Global distribution of carbon monoxide, *J. Geophys. Res.*, 105(D10), 12123, doi:10.1029/1999JD901173, 2000.
- Hooghiemstra, P. B., Krol, M. C., Bergamaschi, P., de Laat, A. T. J., Van der Werf, G. R., Novelli, P. C., Deeter, M. N., Aben, I. and Röckmann, T.: Comparing optimized CO emission estimates using MOPITT or NOAA surface network observations, *J. Geophys. Res.*, 117(D6), doi:DOI: 10.1029/2011JD017043, 2012.
- 1120
- Hourdin, F., Musat, I., Bony, S., Braconnot, P., Codron, F., Dufresne, J.-L., Fairhead, L., Filiberti, M.-A., Friedlingstein, P., Grandpeix, J.-Y., Krinner, G., LeVan, P., Li, Z.-X. and Lott, F.: The LMDZ4 general circulation model: climate performance and sensitivity to parametrized physics with emphasis on tropical convection, *Clim. Dyn.*, 27(7-8), 787–813, doi:10.1007/s00382-006-0158-0, 2006.
- 1125
- Jacob, D.: Introduction to atmospheric chemistry, Princeton University Press., 1999.
- Jiang, Z., Jones, D. B. a., Worden, H. M., Deeter, M. N., Henze, D. K., Worden, J., Bowman, K. W., Brenninkmeijer, C. a. M. and Schuck, T. J.: Impact of model errors in convective transport on CO source estimates inferred from MOPITT CO retrievals, *J. Geophys. Res. Atmos.*, 118(4), 2073–2083, doi:10.1002/jgrd.50216, 2013.
- 1130
- Khalil, M. A. K. and Rasmussen, R. A.: Carbon monoxide in the Earth's atmosphere: indications of a global increase, *Nature*, 332(6161), 242–245, 1988.
- Kim, D.-H., Sexton, J. O. and Townshend, J. R.: Accelerated Deforestation in the Humid Tropics from the 1990s to the 2000s, *Geophys. Res. Lett.*, doi:10.1002/2014GL062777, 2015.
- 1135
- Kopacz, M., Jacob, D. J., Fisher, J. A., Logan, J. A., Zhang, L., Megretskaia, I. A., Yantosca, R. M., Singh, K., Henze, D. K., Burrows, J. P., Buchwitz, M., Khlystova, I., McMillan, W. W., Gille, J. C., Edwards, D. P., Eldering, A., Thouret, V. and Nedelec, P.: Global estimates of CO sources with high resolution by adjoint inversion of multiple satellite datasets (MOPITT, AIRS, SCIAMACHY, TES), *Atmos. Chem. Phys.*, 10(3), 855–876, doi:10.5194/acp-10-855-2010, 2010.
- 1140
- Kurokawa, J., Ohara, T., Morikawa, T., Hanayama, S., Janssens-Maenhout, G., Fukui, T., Kawashima, K. and Akimoto, H.: Emissions of air pollutants and greenhouse gases over Asian regions during 2000–2008: Regional Emission inventory in ASia (REAS) version 2, *Atmos. Chem. Phys.*, 13(21), 11019–11058, doi:10.5194/acp-13-11019-2013, 2013.
- 1145
- Lamarque, J. F., Bond, T. C., Eyring, V., Granier, C., Heil, A., Klimont, Z., Lee, D., Liousse, C., Mieville, A., Owen, B., Schultz, M. G., Shindell, D., Smith, S. J., Stehfest, E., Van Aardenne, J., Cooper, O. R., Kainuma, M., Mahowald, N., McConnell, J. R., Naik, V., Riahi, K. and van Vuuren, D. P.: Historical (1850–2000) gridded anthropogenic and biomass burning emissions of reactive gases and aerosols: methodology and application, *Atmos. Chem. Phys.*, 10(15), 7017–7039, 2010.
- 1150

- van Leeuwen, T. T., Peters, W., Krol, M. C. and van der Werf, G. R.: Dynamic biomass burning emission factors and their impact on atmospheric CO mixing ratios, *J. Geophys. Res. Atmos.*, 118(12), 6797–6815, doi:10.1002/jgrd.50478, 2013.
- 1155 Lelieveld, J., Butler, T. M., Crowley, J. N., Dillon, T. J., Fischer, H., Ganzeveld, L., Harder, H., Lawrence, M. G., Martinez, M., Taraborrelli, D. and Williams, J.: Atmospheric oxidation capacity sustained by a tropical forest., *Nature*, 452(7188), 737–40, doi:10.1038/nature06870, 2008.
- Li, L. and Liu, Y.: Space-borne and ground observations of the characteristics of CO pollution in Beijing, 2000–2010, *Atmos. Environ.*, 45(14), 2367–2372, doi:10.1016/j.atmosenv.2011.02.026, 2011.
- 1160 Logan, J. A., Prather, M. J., Wofsy, S. C. and McElroy, M. B.: Tropospheric Chemistry: A Global Perspective, *J. Geophys. Res.*, (86), 1–45, doi:DOI: 10.1029/JC086iC08p07210, 1981.
- Mao, J., Ren, X., Zhang, L., Van Duin, D. M., Cohen, R. C., Park, J.-H., Goldstein, A. H., Paulot, F., Beaver, M. R., Crounse, J. D., Wennberg, P. O., DiGangi, J. P., Henry, S. B., Keutsch, F. N., Park, C., Schade, G. W., Wolfe, G. M., Thornton, J. A. and Brune, W. H.: Insights into hydroxyl measurements and atmospheric oxidation in a California forest, *Atmos. Chem. Phys.*, 12(17), 8009–8020, doi:10.5194/acp-12-8009-2012, 2012.
- 1165 Meyfroidt, P. and Lambin, E. F.: Global Forest Transition: Prospects for an End to Deforestation, *Annu. Rev. Environ. Resour.*, 36(1), 343–371, doi:10.1146/annurev-environ-090710-143732, 2011.
- Mu, M., Randerson, J. T., van der Werf, G. R., Giglio, L., Kasibhatla, P., Morton, D., Collatz, G. J., DeFries, R. S., Hyer, E. J., Prins, E. M., Griffith, D. W. T., Wunch, D., Toon, G. C., Sherlock, V. and Wennberg, P. O.: Daily and 3-hourly variability in global fire emissions and consequences for atmospheric model predictions of carbon monoxide, *J. Geophys. Res. Atmos.*, 116(D24), doi:10.1029/2011JD016245, 2011.
- 1175 Naik, V., Voulgarakis, A., Fiore, A. M., Horowitz, L. W., Lamarque, J.-F., Lin, M., Prather, M. J., Young, P. J., Bergmann, D., Cameron-Smith, P. J., Cionni, I., Collins, W. J., Dalsøren, S. B., Doherty, R., Eyring, V., Faluvegi, G., Folberth, G. A., Josse, B., Lee, Y. H., MacKenzie, I. A., Nagashima, T., van Noije, T. P. C., Plummer, D. A., Righi, M., Rumbold, S. T., Skeie, R., Shindell, D. T., Stevenson, D. S., Strode, S., Sudo, K., Szopa, S. and Zeng, G.: Preindustrial to present-day changes in tropospheric hydroxyl radical and methane lifetime from the Atmospheric Chemistry and Climate Model Intercomparison Project (ACCMIP), *Atmos. Chem. Phys.*, 13(10), 5277–5298, doi:10.5194/acp-13-5277-2013, 2013.
- 1180 Novelli, P. C., Masarie, K. A., Lang, P. M., Hall, B. D., Myers, R. C. and Elkins, J. W.: Reanalysis of tropospheric CO trends: Effects of the 1997–1998 wildfires, *J. Geophys. Res. Atmos.*, 108(D15), 4464, doi:10.1029/2002JD003031, 2003.
- Patra, P. K., Houweling, S., Krol, M., Bousquet, P., Belikov, D., Bergmann, D., Bian, H.,

- 1190 Cameron-Smith, P., Chipperfield, M. P., Corbin, K., Fortems-Cheiney, A., Fraser, A., Gloor, E., Hess, P., Ito, A., Kawa, S. R., Law, R. M., Loh, Z., Maksyutov, S., Meng, L., Palmer, P. I., Prinn, R. G., Rigby, M., Saito, R. and Wilson, C.: TransCom model simulations of CH₄ and related species: linking transport, surface flux and chemical loss with CH₄ variability in the troposphere and lower stratosphere, *Atmos. Chem. Phys.*, 11(24), 12813–12837, doi:10.5194/acp-11-12813-2011, 2011.
- 1195 Pétron, G.: Inverse modeling of carbon monoxide surface emissions using Climate Monitoring and Diagnostics Laboratory network observations, *J. Geophys. Res.*, 107(D24), 4761, doi:10.1029/2001JD001305, 2002.
- Pétron, G., Granier, C., Khattatov, B., Yudin, V., Lamarque, J.-F., Emmons, L., Gille, J. and Edwards, D. P.: Monthly CO surface sources inventory based on the 2000–2001 MOPITT satellite data, *Geophys. Res. Lett.*, 31(21), L21107, doi:10.1029/2004GL020560, 2004.
- 1200 Pison, I., Bousquet, P., Chevallier, F., Szopa, S. and Hauglustaine, D.: Multi-species inversion of CH₄, CO and H₂ emissions from surface measurements, *Atmos. Chem. Phys.*, 9(14), 5281–5297, doi:10.5194/acp-9-5281-2009, 2009.
- 1205 Poulter, B., Frank, D., Ciais, P., Myneni, R. B., Andela, N., Bi, J., Broquet, G., Canadell, J. G., Chevallier, F., Liu, Y. Y., Running, S. W., Sitch, S. and van der Werf, G. R.: Contribution of semi-arid ecosystems to interannual variability of the global carbon cycle, *Nature*, 509(7502), 600–603, doi:10.1038/nature13376, 2014.
- 1210 Randerson, J. T., Chen, Y., van der Werf, G. R., Rogers, B. M. and Morton, D. C.: Global burned area and biomass burning emissions from small fires, *J. Geophys. Res.*, 117(G4), G04012, doi:10.1029/2012JG002128, 2012.
- Rayner, P. J. and O'Brien, D. M.: The utility of remotely sensed CO₂ concentration data in surface source inversions, *Geophys. Res. Lett.*, 28(1), 175–178, doi:10.1029/2000GL011912, 2001.
- 1215 Reuter, M., Buchwitz, M., Hilboll, A., Richter, A., Schneising, O., Hilker, M., Heymann, J., Bovensmann, H. and Burrows, J. P.: Decreasing emissions of NO_x relative to CO₂ in East Asia inferred from satellite observations, *Nat. Geosci.*, 7, doi:10.1038/ngeo2257, 2014.
- 1220 Rohrer, F., Lu, K., Hofzumahaus, A., Bohn, B., Brauers, T., Chang, C.-C., Fuchs, H., Häseler, R., Holland, F., Hu, M., Kita, K., Kondo, Y., Li, X., Lou, S., Oebel, A., Shao, M., Zeng, L., Zhu, T., Zhang, Y. and Wahner, A.: Maximum efficiency in the hydroxyl-radical-based self-cleansing of the troposphere, *Nat. Geosci.*, 7(8), 559–563, doi:10.1038/ngeo2199, 2014.
- 1225 Shindell, D. T., Faluvegi, G., Stevenson, D. S., Krol, M. C., Emmons, L. K., Lamarque, J.-F., Pétron, G., Dentener, F. J., Ellingsen, K., Schultz, M. G., Wild, O., Amann, M., Atherton, C. S., Bergmann, D. J., Bey, I., Butler, T., Cofala, J., Collins, W. J., Derwent, R. G., Doherty, R. M., Drevet, J., Eskes, H. J., Fiore, A. M., Gauss, M., Hauglustaine, D. A., Horowitz, L. W., Isaksen, I. S. A., Lawrence, M. G., Montanaro, V., Müller, J.-F., Pitari, G., Prather, M. J.,

- Pyle, J. A., Rast, S., Rodriguez, J. M., Sanderson, M. G., Savage, N. H., Strahan, S. E., Sudo, K., Szopa, S., Unger, N., van Noije, T. P. C., Zeng, G., G, F. and D S, S.: Multimodel simulations of carbon monoxide: Comparison with observations and projected near-future changes, *J. Geophys. Res.*, 111(D19), D19306, doi:10.1029/2006JD007100, 2006.
- 1230 De Smedt, I., Stavrou, T., Müller, J.-F., van der A, R. J. and Van Roozendael, M.: Trend detection in satellite observations of formaldehyde tropospheric columns, *Geophys. Res. Lett.*, 37(18), doi:10.1029/2010GL044245, 2010.
- Stavrou, T. and Müller, J.-F.: Grid-based versus big region approach for inverting CO emissions using Measurement of Pollution in the Troposphere (MOPITT) data, *J. Geophys. Res.*, 111(D15), D15304, doi:10.1029/2005JD006896, 2006.
- 1235 Stein, O., Schultz, M. G., Bouarar, I., Clark, H., Huijnen, V., Gaudel, A., George, M. and Clerbaux, C.: On the wintertime low bias of Northern Hemisphere carbon monoxide found in global model simulations, *Atmos. Chem. Phys.*, 14(17), 9295–9316, doi:10.5194/acp-14-9295-2014, 2014.
- 1240 Stocker, T. F., Qin, D., Plattner, G.-K., Tignor, M., Allen, S. K., Boschung, J., Nauels, A., Xia, Y., Bex, V., Midgley, P. M. and others: *Climate Change 2013. The Physical Science Basis. Working Group I Contribution to the Fifth Assessment Report of the Intergovernmental Panel on Climate Change-Abstract for decision-makers.*, 2013.
- Thompson, A. M.: The Oxidizing Capacity of the Earth's Atmosphere: Probable Past and
1245 Future Changes, *Science (80-.)*, 256(5060), 1157–1165, doi:10.1126/science.256.5060.1157, 1992.
- Tohjima, Y., Kubo, M., Minejima, C., Mukai, H., Tanimoto, H., Ganshin, A., Maksyutov, S., Katsumata, K., Machida, T. and Kita, K.: Temporal changes in the emissions of CH₄ and CO from China estimated from CH₄ / CO₂ and CO / CO₂ correlations observed at Hateruma
1250 Island, *Atmos. Chem. Phys.*, 14(3), 1663–1677, doi:10.5194/acp-14-1663-2014, 2014.
- Wang, R., Tao, S., Shen, H., Huang, Y., Chen, H., Balkanski, Y., Boucher, O., Ciais, P., Shen, G., Li, W., Zhang, Y., Chen, Y., Lin, N., Su, S., Li, B., Liu, J. and Liu, W.: Trend in global black carbon emissions from 1960 to 2007., *Environ. Sci. Technol.*, 48(12), 6780–7, doi:10.1021/es5021422, 2014.
- 1255 Warner, J., Carminati, F., Wei, Z., Lahoz, W. and Attié, J.-L.: Tropospheric carbon monoxide variability from AIRS under clear and cloudy conditions, *Atmos. Chem. Phys.*, 13(24), 12469–12479, doi:10.5194/acp-13-12469-2013, 2013.
- van der Werf, G. R., Randerson, J. T., Giglio, L., Collatz, G. J., Kasibhatla, P. S. and Arellano, A. F.: Interannual variability in global biomass burning emissions from 1997 to
1260 2004, *Atmos. Chem. Phys.*, 6(11), 3423–3441, doi:10.5194/acp-6-3423-2006, 2006.
- Van der Werf, G. R., Randerson, J. T., Giglio, L., Collatz, G. J., Mu, M., Kasibhatla, P. S., Morton, D. C., DeFries, R. S., Jin, Y. and van Leeuwen, T. T.: Global fire emissions and the

contribution of deforestation, savanna, forest, agricultural, and peat fires (1997–2009), *Atmos. Chem. Phys.*, 10(23), 11707–11735, 2010.

1265 Worden, H. M., Deeter, M. N., Frankenberg, C., George, M., Nichitiu, F., Worden, J., Aben, I., Bowman, K. W., Clerbaux, C., Coheur, P.-F., de Laat, A. T. J., Detweiler, R., Drummond, J. R., Edwards, D. P., Gille, J. C., Hurtmans, D., Luo, M., Martínez-Alonso, S., Massie, S., Pfister, G. and Warner, J. X.: Decadal record of satellite carbon monoxide observations, *Atmos. Chem. Phys.*, 13(2), 837–850, 2013.

1270 Yevich, R. and Logan, J. A.: An assessment of biofuel use and burning of agricultural waste in the developing world, *Global Biogeochem. Cycles*, 17(4), doi:10.1029/2002GB001952, 2003.

Yoon, J. and Pozzer, A.: Model-simulated trend of surface carbon monoxide for the 2001–2010 decade, *Atmos. Chem. Phys.*, 14(19), 10465–10482, doi:10.5194/acp-14-10465-2014, 2014.

1275 Zellweger, C., Hüglin, C., Klausen, J., Steinbacher, M., Vollmer, M. and Buchmann, B.: Inter-comparison of four different carbon monoxide measurement techniques and evaluation of the long-term carbon monoxide time series of Jungfraujoch, *Atmos. Chem. Phys.*, 9(11), 3491–3503, doi:10.5194/acp-9-3491-2009, 2009.

1280

Tables

Table 1. Prior datasets for the sources and sinks of CO. Mean annual sums are calculated for the period from 2002 to 2011. The global annual prior error budgets are reported and TransCom-OH field is used.

Sectors	Mean Annual Sum (Tg yr ⁻¹)	Dataset/ Model	References
Sources:			
Biomass burning	327	GFEDv3.1	Van der Werf et al., 2010
Anthropogenic Emissions	588	MACCity	Lamarque et al., 2010
Ocean	54	PISCES	Updated from Aumont et al. 2006
Sum of surface emissions	969±180⁽¹⁾		
CO			
Oxidation from NMVOC	335±43 ⁽²⁾	LMDz-INCA	Folberth et al. 2006
Oxidation from CH ₄	885±92 ⁽³⁾		
Sum of chemical sources	1220		
Sinks:			
Oxidation by OH	2197	TransCom-OH	Patra et al. 2011

Deleted: Belattaf

Deleted: 12

5

- (1) The uncertainty represents the SD of the global annual error budgets in the prior CO emissions in the inversion configuration.
- (2) The SD is calculated into the equivalent CO amount from global annual error budgets of the pre-calculated CH₂O production fields.
- (3) The SD is calculated into the equivalent CO amount from global annual error budgets of the prior CH₄ emissions assuming they are all oxidized into CO in a single step. The prior CH₄ emission (506 TgCO yr⁻¹) datasets are detailed in Cressot et al. (2014).

10

15

Table 2. Summary of CO model-data comparison and trend analysis for MOPITT satellite retrievals, surface station observations and corresponding prior/posterior modelling. Trends for each region (in the unit of ppb yr⁻¹) are the mean values for all the grids whose trends are significant at 95% confidence level. The percentages of significant trends are also given per model grid for positive (+) and negative (-) respectively.

REGIONS	MOPITT		Surface		N	MOPITT column trends									N	Surface station trends								
	Prior Bias	Post Bias	Prior Bias	Post Bias		Observation			Prior mod			Posterior mod				Observation			Prior mod			Posterior mod		
	(ppb)					Trend	+	-	Trend	+	-	Trend	+	-		Trend	+	-	Trend	+	-	Trend	+	-
BONA	-14.1	0.7	-20.8	20.5	210	-0.84	99	-0.46	95	-0.88	99	2	-2.51	100	-1.46	100	-2.96	100						
USA	-16.7	-3.1	-20.4	20.1	108	-0.82	97	-0.41	96	-1.08	100	3	-1.67	67	-1.13	100	-3.30	100						
NHSA	-10.0	-3.0			74	-0.61	84	-0.19	8	53	-0.68	100	0											
SHSA	-14.2	0.2			160	-0.59	58	0.38	41		-0.56	67	0											
NHAF	-15.0	-2.0	-20.0	6.8	211	-0.45	7	55	-0.38	85	-0.73	95	1	-0.90	100	-0.73	100	-1.04	100					
SHAF	-16.5	0.5	-1.5	13.6	96	-0.57	75	0.07	27	11	-0.64	96	1	-0.78	100	0.42	100	-0.48	100					
WSEU	-16.1	0.3	-36.7	18.7	106	-1.00	100	-0.49	100	-1.12	100	6	-2.73	100	-2.05	100	-3.51	100						
ESEU	-16.8	0.4			108	-0.77	100	-0.40	100	-0.93	100	0												
BOAS	-17.3	1.0			227	-0.92	99	-0.51	92	-1.02	99	0												
MIDE	-16.5	-2.9			64	-0.57	100	-0.30	100	-0.88	100	0												
SCAS	-12.0	-0.3			80	-0.65	63	-0.30	4	38	-0.92	100	0											
SEAS	-20.1	-3.6	-30.6	22.6	129	-1.23	97	0.13	19	24	-1.35	99	3	-1.76	100	-1.83	100	-3.78	100					
AUST	-15.5	-1.7	-6.4	15.4	105	-0.62	100	0.17	28		-0.78	100	3	-0.34	67	--		-1.18	67					
INDO	-3.8	0.2			64	-1.20	98	-0.84	28	-1.03	98	0												
OCEAN	-11.9	-0.2	-15.1	9.6	3092	-0.72	96	-0.07	22	25	-0.67	97	27	-1.23	4	89	-1.00	7	59	-1.46	89			

Table 3. Fitness of CH₄ and MCF observations assimilated in the inversion.

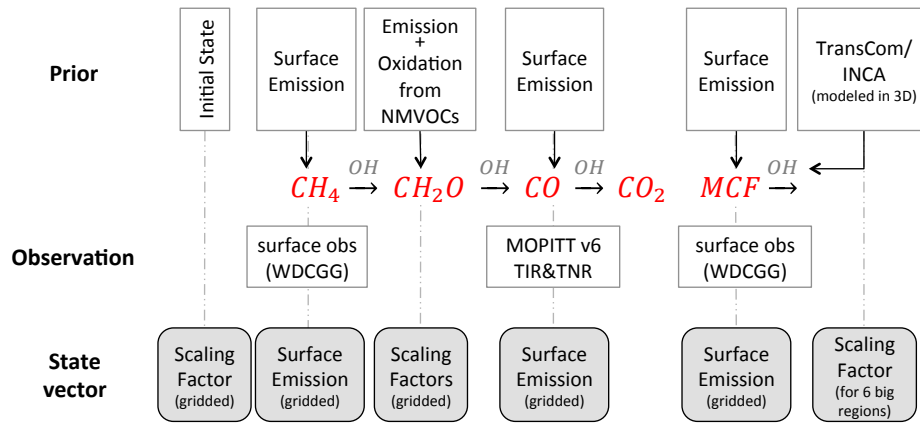
Region	OH-type	CH ₄ (ppb)				MCF (ppt)			
		Mean bias		Residual square		Mean bias		Residual square	
		<i>prior</i>	<i>posterior</i>	<i>prior</i>	<i>posterior</i>	<i>prior</i>	<i>posterior</i>	<i>prior</i>	<i>posterior</i>
NH(30-90)	<i>TransCom</i>	<u>20.6</u>	<u>2.4</u>	<u>749.6</u>	<u>22.2</u>	<u>1.02</u>	<u>-0.02</u>	<u>1.14</u>	<u>0.05</u>
	<i>INCA</i>	<u>-21.0</u>	<u>2.5</u>	<u>658.1</u>	<u>20.1</u>	<u>0.44</u>	<u>-0.09</u>	<u>0.28</u>	<u>0.07</u>
NH(0-30)	<i>TransCom</i>	<u>15.8</u>	<u>1.5</u>	<u>452.6</u>	<u>19.1</u>	<u>0.90</u>	<u>-0.20</u>	<u>0.91</u>	<u>0.16</u>
	<i>INCA</i>	<u>-21.1</u>	<u>-0.1</u>	<u>564.9</u>	<u>13.9</u>	<u>0.40</u>	<u>-0.20</u>	<u>0.21</u>	<u>0.11</u>
SH(0-30)	<i>TransCom</i>	<u>10.9</u>	<u>-2.4</u>	<u>222.1</u>	<u>20.1</u>	<u>1.19</u>	<u>0.09</u>	<u>1.61</u>	<u>0.13</u>
	<i>INCA</i>	<u>-14.3</u>	<u>-4.0</u>	<u>264.9</u>	<u>29.5</u>	<u>0.88</u>	<u>0.23</u>	<u>0.94</u>	<u>0.15</u>
SH(30-90)	<i>TransCom</i>	<u>14.4</u>	<u>0.2</u>	<u>308.3</u>	<u>4.7</u>	<u>0.88</u>	<u>-0.24</u>	<u>0.90</u>	<u>0.17</u>
	<i>INCA</i>	<u>-7.9</u>	<u>-0.4</u>	<u>96.6</u>	<u>5.7</u>	<u>0.60</u>	<u>-0.06</u>	<u>0.46</u>	<u>0.07</u>

25

Figures

Fig. 1. Schematics of the input information provided to the inversion and of the inversion state

30 vector.



35 | **Fig. 2. Distribution of prior budget terms for CO.** Annual mean values per model grid (2.5° latitude \times 3.75° longitude) from 2002 to 2011 are shown. (a) Surface CO emissions, (b) Relative percentages of CO emissions from biomass burning over land, (c) Atmospheric CO productions from CH_4 and NMVOCs, (d) Atmospheric CO chemical sinks. The chemical productions and sinks are calculated with TransCom-OH.

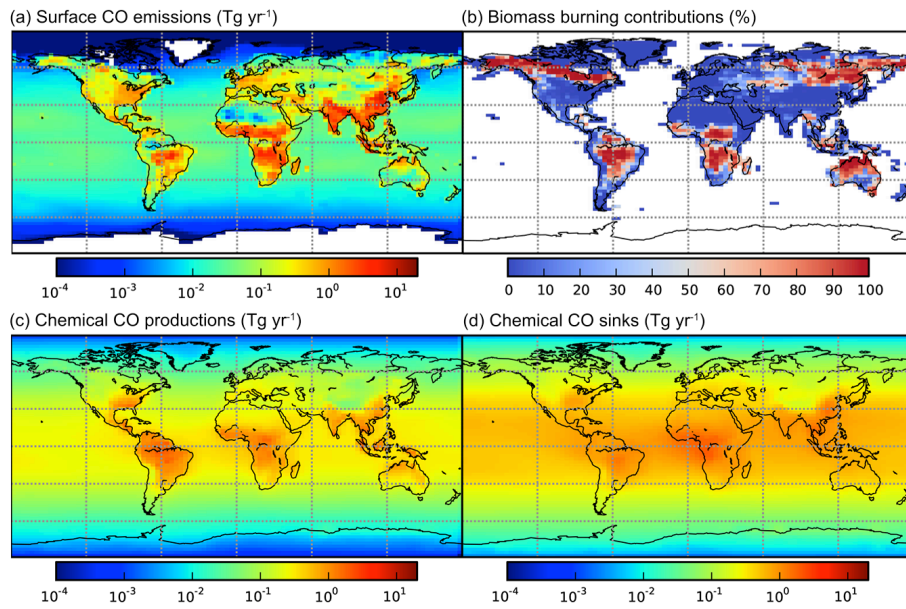


Fig. 3. Spatial and vertical distribution of OH concentrations in TransCom and INCA and their relative differences. The TransCom OH is interpolated from its original 60 pressure levels into the LMDz 19 eta- pressure levels.

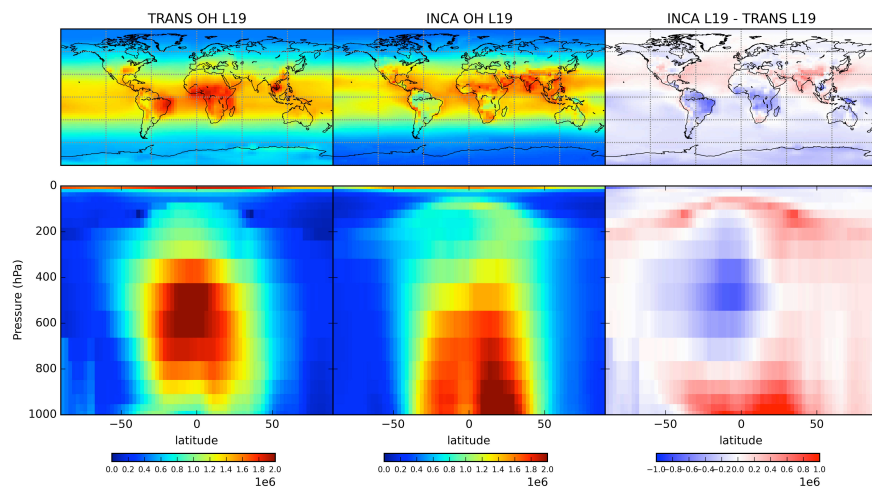
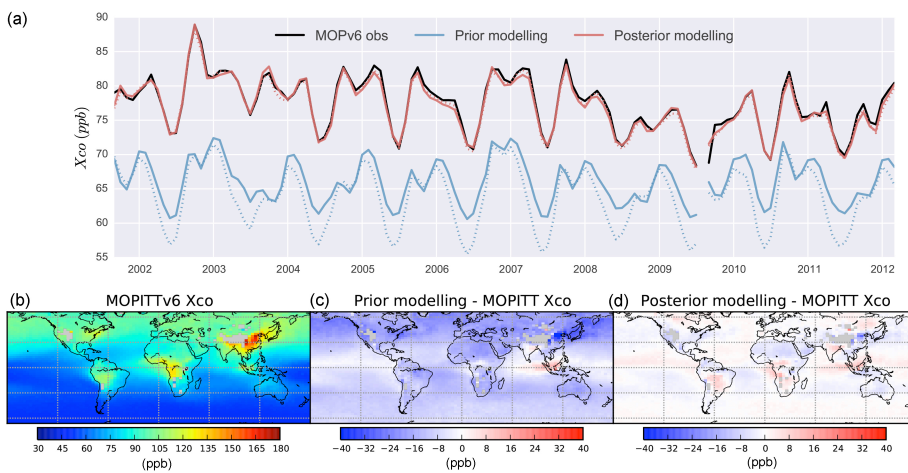
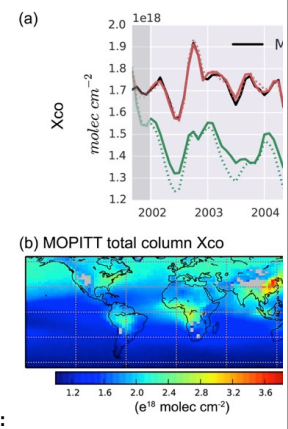


Fig. 4. Time series and spatial distributions of CO total column (X_{CO}). (a) Time series of global monthly mean mole fraction in CO column. The black line represents satellite observation of MOPITTv6 X_{CO} , the blue (red) lines represent the prior (posterior) simulations. Solid lines represent the control version with TransCom-OH, and dotted lines represent the test with INCA-OH. (b) Distribution of multi-year mean annual X_{CO} of MOPITTv6 retrieval. (c) Mean annual difference between the prior simulation and MOPITT. (d) Mean annual difference between the posterior simulation and MOPITT. Simulations shown in c and d used TransCom-OH. The results with INCA-OH show similar spatial distributions and are not shown here.



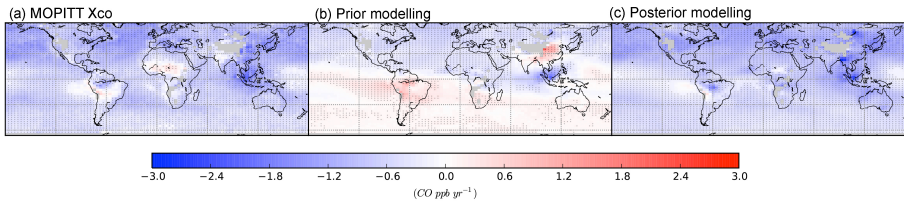
Deleted: 3
 Deleted: X_{CO}
 Deleted: green

55



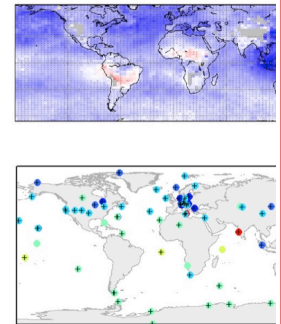
Deleted:

Fig. 5. Distribution of CO column mixing ratio trends from 2002 to 2011 in (a) MOPITTv6 retrievals, (b) the prior simulation and (c) the posterior simulation. Black crosses indicate significance at 95% confidence level.



Deleted: Fig. 4. Time series of monthly mean CO misfit between forward (green) or posterior (red) modelling against surface measurements in each latitudinal zone. The shaded areas represent the spatial standard deviation among the sites in each zone. ... [1]

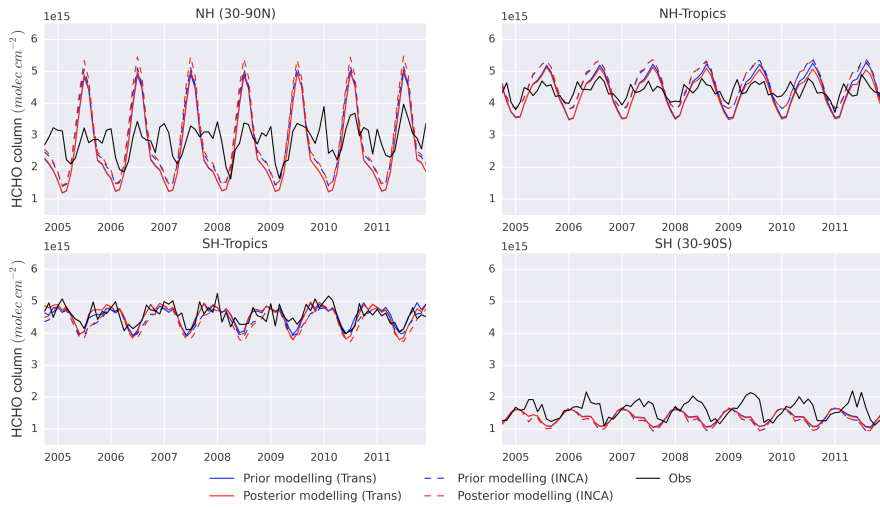
Deleted: The lower section shows the CO concentration trends at the surface stations from WGCDD and corresponding forward/posterior modelling trends at those stations. Black crosses indicate significance at 95% confidence level. Difference colour bars are used for X_{CO} and surface CO concentrations, and the two values are not directly comparable.



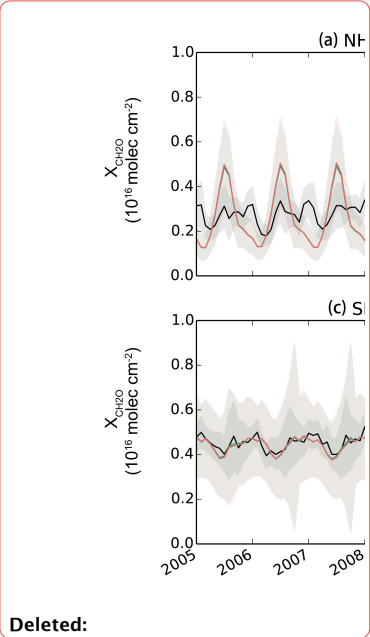
Deleted:

Fig. 6. Time series of CH₂O total column averaged by latitudinal bands. The black lines indicate the CH₂O total column from SAO OMI retrievals, green lines indicate prior simulations, and red lines indicate posterior simulations.

85



Deleted: Shading areas show the standard deviation within a latitudinal band. The forward and posterior simulations nearly overlay each other.

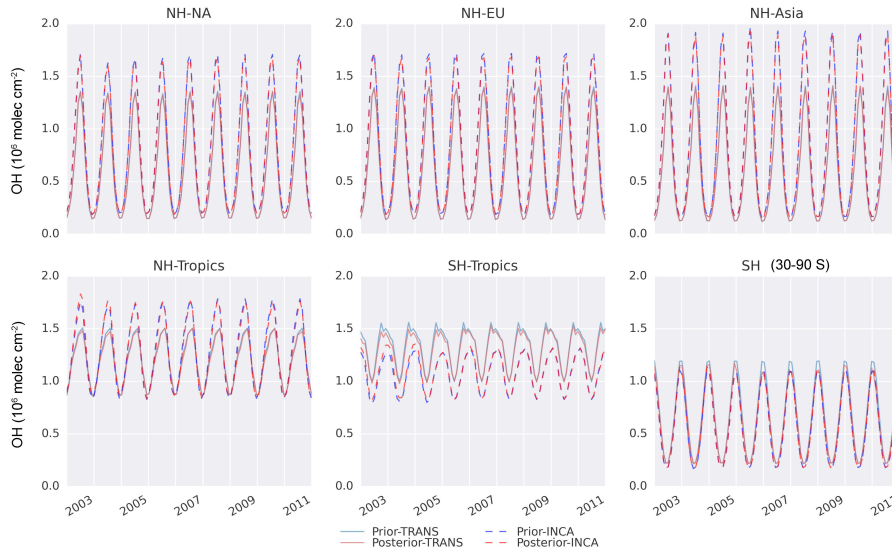


Deleted:

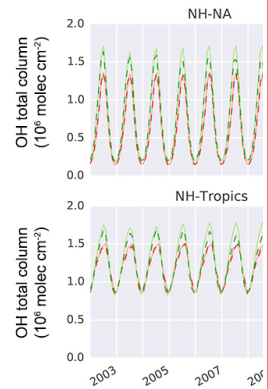
Fig. 7. ~~Column~~ mean OH concentrations in the prior and posterior. The results are shown for the 6 big regions in which OH is optimized.

Deleted: Regional volume-weighted monthly

95



100



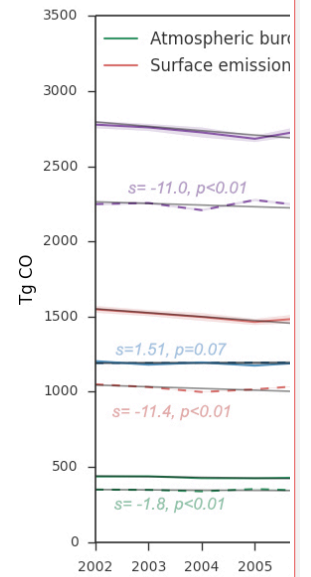
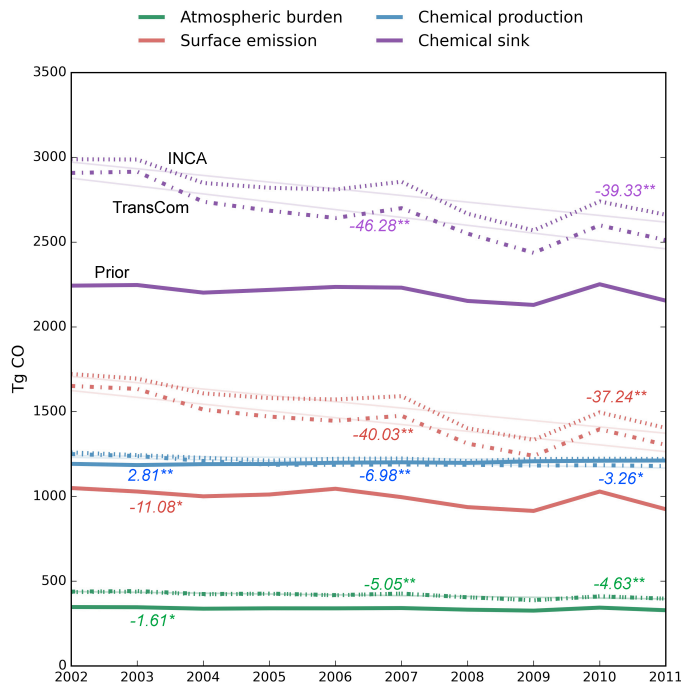
Deleted:

10

105

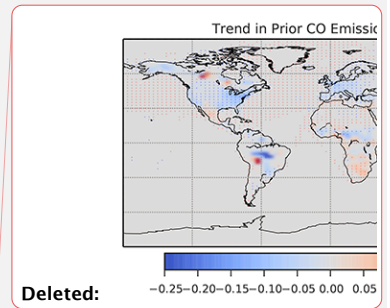
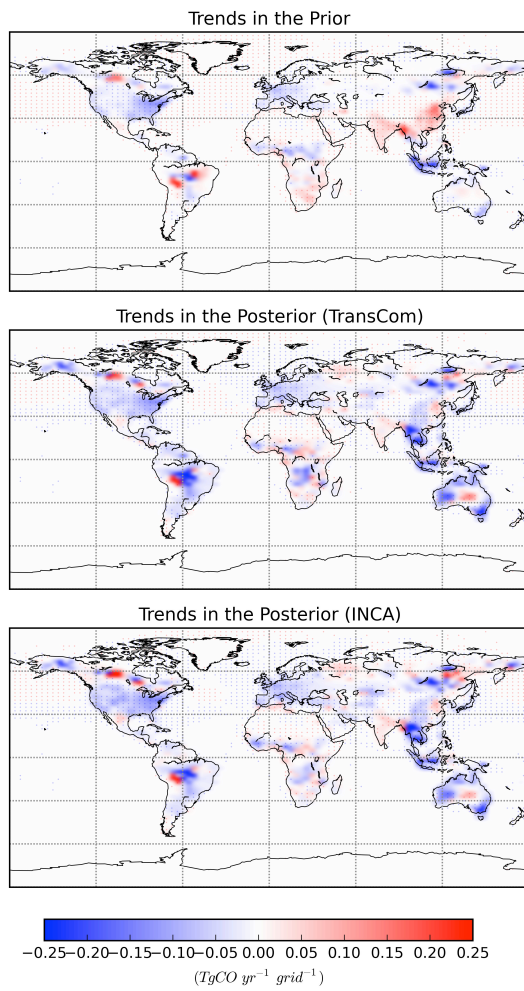
Fig. 8. Time series of global mean annual CO budget changes from 2002 to 2011. Each component is shown in a different colour. Solid lines indicate the prior values (mean values of the two OH fields are shown for the prior chemical CO production and sink). Dash-dot lines indicate posterior with TransCom OH and dotted lines represent posterior with INCA-OH. With the order from left to right, the linear slopes of the prior, the posterior with TransCom-OH and the posterior of INCA-OH are denoted successively if the trend is statistically significant. * denotes 95% confidence level and ** denotes 99% confidence level.

110



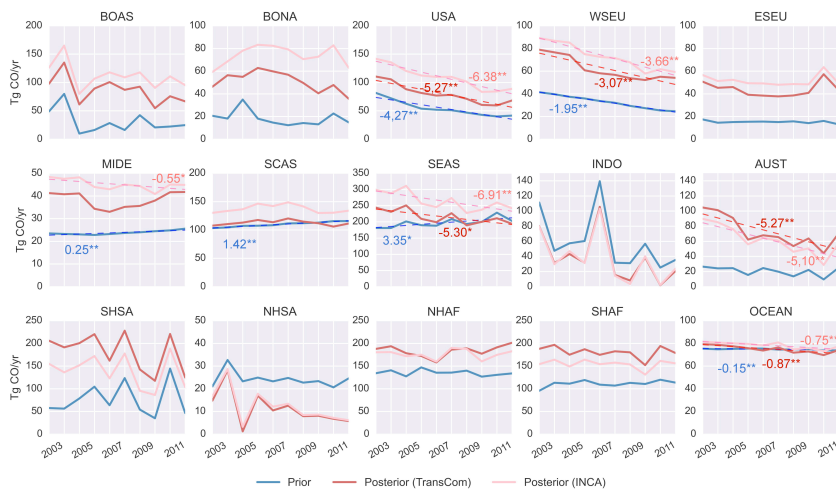
Deleted:

Fig. 9. Trends distributions of CO surface emissions in the prior and in the posterior from 2002 to 2011.



Deleted:

Fig. 10. Annual prior (blue) and posterior (red) CO emissions in each sub-region from 2002 to 2011. The dash lines represent linear regressions, beside which s denotes the linear slope and p denotes the p-value for the regression. The notation for the sub-regions are listed as follows and the extent of each region is shown in Fig. A.1. BOAS - Boreal Asia, BONA - Boreal North America, USA - USA, WSEU - West Europe, ESEU - East Europe, MIDE - Middle East, SCAS - South Central Asia, SEAS - South East Asia, INDO- Indonesia, AUST - Australia, NHSA- North Hemisphere South America, SHSA - South Hemisphere South America, NHAF - North Hemisphere Africa, SHAF - South Hemisphere Africa, OCEAN - all ocean emissions both biogenic and anthropogenic emissions.



Deleted: green

Deleted: S



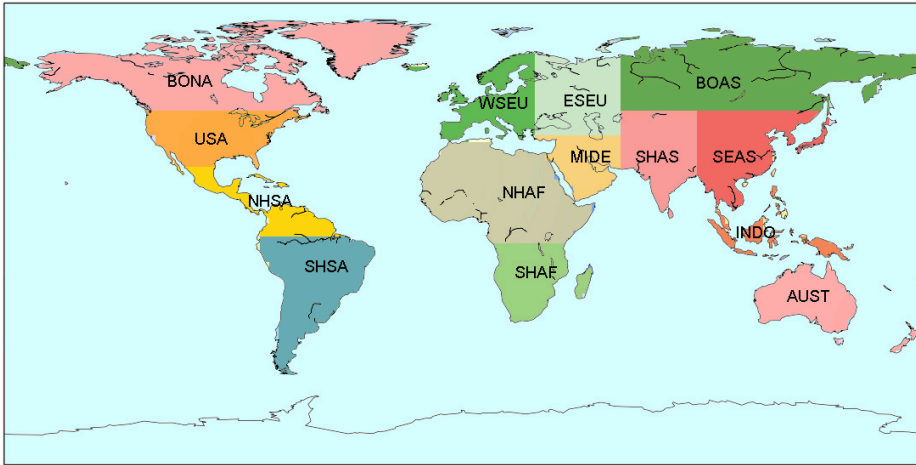
Deleted:

125

130

135

Fig. A1. Sub-region extent.



Deleted: S